

St. John's University

St. John's Scholar

Theses and Dissertations

2021

**DEVELOPMENT OF NANOLIPOSOMES FOR THE TREATMENT OF
BRAF V600E MUTATED PARENT AND VEMURAFENIB-RESISTANT
MELANOMA**

Yige Fu

Follow this and additional works at: https://scholar.stjohns.edu/theses_dissertations



Part of the [Pharmacy and Pharmaceutical Sciences Commons](#)

**DEVELOPMENT OF NANOLIPOSOMES FOR THE TREATMENT OF BRAF
V600E MUTATED PARENT AND VEMURAFENIB-RESISTANT MELANOMA**

A dissertation submitted in partial fulfillment of the
requirements for the degree of

DOCTOR OF PHILOSOPHY

to the faculty of the

DEPARTMENT OF GRADUATE DIVISION
of
COLLEGE PHARMACY AND HEALTH SCIENCES

at

ST. JOHN'S UNIVERSITY

New York

by

YIGE FU

Date Submitted: _____

Date Approved: _____

YIGE FU

KETANKUMAR PATEL, PhD

© Copyright by YIGE FU 2021

All Rights Reserved

ABSTRACT

DEVELOPMENT OF NANOLIPOSOMES FOR THE TREATMENT OF BRAF^{V600E} MUTATED PARENT AND VEMURAFENIB-RESISTANT MELANOMA

YIGE FU

Melanoma is one of the most aggressive and deadliest types of skin cancer. Currently, off-target toxicities and the rapid resistance development of metastatic melanoma mainly restrict the efficiency of the treatments. This thesis presents efforts towards developing liposomes to address current problems of BRAF-mutant metastatic melanoma.

EphA2-Receptor Targeted PEGylated Nanoliposomes for the Treatment of BRAF^{V600E} Mutated Parent and Resistant Melanoma

In order to address off-target toxicities of the targeted therapy of MEK inhibitor trametinib (TMB), we developed a physically stable EphrinA1-mimicking peptide (YSA) anchored TMB-loaded PEGylated nanoliposomes (YTPLs). The YTPLs were evaluated in BRAF^{V600E}-mutated parent cell lines (A375 and SK-MEL-28) and vemurafenib-resistant cell lines (A375R and SK-MEL-28R). A differential scanning calorimetry (DSC) study confirmed that TMB was retained in a solubilized state within the lipid bilayers. No burst release was observed of TMB in 24 h and negligible hemolysis was observed at therapeutic concentrations of TMB. YTPL showed higher intracellular uptake in parental cell lines compared to vemurafenib-resistant cell lines. Western blot analysis and a cytotoxicity study with the EphA2 inhibitor confirmed a reduction in EphA2 expression in resistant cell lines. Thus, YTPLs can be useful for metastatic melanoma-specific delivery of TMB.

Development of BRD4 PROTAC and anti-fibrotic agent co-loaded PEGylated Nanoliposome for BRAF inhibitor resistant Melanoma

In the present study, we proposed a new treatment strategy for the treatment of vemurafenib-resistant melanoma by targeting to both cancer cells and tumor stroma. A BRD4 proteolysis targeting chimera (ARV-825) and nintedanib co-loaded PEGylated nanoliposomes (ARNIPL) were developed in a synergistic cytotoxic ratio against vemurafenib-resistant melanoma. Both the molecules have extremely poor aqueous solubility. Citric acid was used to improve the loading of both the molecules in ARNIPL. ARNIPL with mean particle size 111.1 ± 6.55 nm exhibited more than 90% encapsulation efficiency (EE) for both the drugs and was found to be physically stable for a month. Both the molecules and ARNIPL showed significantly higher cytotoxicity, apoptosis and downregulation of target proteins BRD4 and c-Myc in vemurafenib-resistant cell line (A375R). Vasculogenic mimicry and clonogenic potential of A375R were significantly inhibited by ARNIPL. Tumor growth inhibition in 3D spheroid of A375R and 3D spheroid of co-culture of A375R+Dermal fibroblasts model with reduction of TGF- β 1 was observed with ARNIPL treatment. Therefore, ARNIPL could be a novel therapeutic approach for the treatment of vemurafenib-resistant melanoma.

ACKNOWLEDGMENTS

Initially I would like to express my sincere gratitude to my mentor, Ketankumar Patel, who provided such expert guidance and advice throughout my PhD journey. He possesses an amazing amount of expertise and knowledge that motivated and helped me in all the time of research. Besides my advisor, I would like to thank the rest of my thesis committee: Prof. Dr. Zhe-sheng Chen, Dr. Vikas V. Dukhande, Dr. Vivek Gupta, Dr. and Dr. Nitesh Kunda for their insightful comments and encouragement to widen my research from various perspectives. Moreover, I would like to thank Dr. Sandra E. Reznik for serving as my defense chair. I also express my thanks to my labmates: Aishwarya L. Saraswat, Drishti Rathod, Pavan Kumar Nukala, Manali Patki, Siddhant Palekar, Richa Vartak, Tasneem Gandhi. I'm glad to work with all of you and have your company. I would like to thank my friends especially Zenghui Wei and Chaoyun Cai. I really appreciate the encouragement and company that you gave to me throughout my time at St. John's University. I would also express my sincere thanks to department of pharmaceutical sciences for providing financial support since my second semester. I would like to thank Outrun the Sun for providing financial support for the first part of my thesis project. Last but not the least, I am extremely grateful to my family for supporting me spiritually throughout writing this thesis and my life in general.

TABLE OF CONTENTS

1 Introduction	1
1.1 Melanoma	1
1.2 Treatment approaches	4
1.3 Tumor stroma in melanoma	7
1.4 Liposomes	9
1.5 Literature review	11
2 Purpose of Study	15
3 EphA2-Receptor Targeted PEGylated Nanoliposomes for the Treatment of BRAF ^{V600E} Mutated Parental and Resistant Melanoma	17
3.1 Drug (Trametinib)	17
3.2 Erythropoietin-producing hepatocellular (EphA2) receptor	19
3.3 Materials	20
3.4 Methods	21
3.4.1 Analytical Method	21
3.4.2 Cell Culture	22
3.4.3 Preparation of Liposomes	23
3.4.4 Characterization of liposomes	24
3.4.5 Stability Study	25
3.4.6 Freeze Drying of Liposomes	26
3.4.7 Differential Scanning Calorimetry (DSC) Thermograms of TMB and TPL	27
3.4.8 <i>In Vitro</i> Release Study	28

3.4.9 <i>In Vitro</i> Hemolysis Study	29
3.4.10 Plasma-to-Blood Ratio	30
3.4.11 Cellular Uptake of Liposomes	31
3.4.12 <i>In Vitro</i> Cytotoxicity Test	32
3.4.13 Western Blot Assay	33
3.4 Results and Discussion	34
3.4.1 Analytical Method	34
3.4.2 Preparation of TMB-Loaded PEGylated Liposomes	35
3.4.3 Particle Size and Zeta Potential	37
3.4.4 Stability of Liposomes	39
3.4.5 Freeze Drying of Liposomes	41
3.4.6 DSC Thermograms of TMB and TPL	44
3.4.7 Drug Release Study	46
3.4.8 <i>In Vitro</i> Hemolysis Study and Plasma to Blood Ratio	48
3.4.9 Uptake Study	50
3.4.10 <i>In Vitro</i> Cytotoxicity Test	52
3.4.11 Western Analysis	55
4 Development of Dual ARV-825 and Nintedanib - Loaded Nano-liposome for synergistic efficacy in Vemurafenib-resistant Melanoma	56
4.1 Drug	56
4.1.1 ARV-825	56
4.1.2 Nintedanib	58
4.1.3 Galunisertib	60

4.1.4 Pirfenidone	62
4.2 Materials	64
4.3 Methods	65
4.3.1 Analytical Method (HPLC method development)	65
4.3.2 Enzyme Linked Immunosorbent Assay.....	66
4.3.3 Cell viability assay and effect of drug combination.....	67
4.3.4 Preparation of ARNIPL	68
4.3.5 Characterization of ARNIPL	69
4.3.6 Stability study	70
4.3.7 <i>In Vitro</i> Release Study	71
4.3.8 Clonogenic assay	72
4.3.9 Vasculogenic mimicry	73
4.3.10 Flow cytometry for apoptosis analysis	74
4.3.11 Determination of ARNIPL Efficacy in 3D Spheroids.....	75
4.3.11.1 Development and characterization of 3D multicellular tumor spheroids.....	75
4.3.11.2 3D cell viability study	76
4.3.11.3 3D spheroid live & dead cell imaging.....	77
4.4 Results and Discussion	78
4.4.1 Analytical Method (HPLC)	78
4.4.2 Enzyme Linked Immunosorbent Assay.....	79
4.4.3 Cell viability assay and effect of drug combination.....	81
4.4.4 Characterization.....	84
4.4.5 Stability study	86

4.4.6	<i>In Vitro</i> Release Study	88
4.4.7	Clonogenic assay	90
4.4.8	Vasculogenic mimicry	93
4.4.9	Apoptosis assay	95
4.4.10	Determination of ARNIPL Efficacy in 3D Spheroids	97
4.4.10.1	Development and characterization of 3D multicellular tumor spheroids	97
4.4.10.2	3D cell viability study	102
4.4.10.3	3D spheroid live & dead cell imaging	104
5	Limitations	106
6	Summary	108
7	Significance and future perspectives	110
	References	111

LIST OF TABLES

Table 1. FDA approved drugs for targeting MAPK pathway of BRAF ^{V600E} mutated melanoma	6
Table 2. Trametinib drug profile	18
Table 3. Methods for the preparation of trametinib (TMB)-loaded PEGylated liposomes (TPL).....	36
Table 4. Particle size and zeta potential of YSA-anchored TMB-loaded nanoliposomes (YTPL) and TMB-loaded nanoliposomes (TPL) after freeze drying.....	43
Table 5. <i>In vitro</i> hemolysis study of TPL at various TMB concentrations.....	49
Table 6. <i>In vitro</i> cytotoxicity of TMB, TPL, and YTPL in A375 and SK-MEL-28.....	53
Table 7. ARV-825 drug profile	57
Table 8. Nintedanib drug profile	59
Table 9. Galunisertib drug profile.....	61
Table 10. Pirfenidone drug profile.....	63
Table 11. <i>In vitro</i> cytotoxicity of Ni, ARV alone and in the liposome in A375.....	83
Table 12. Particle size, zeta potential and entrapment efficiency of ARNIPL	85
Table 13. Clonogenic Assay: Surviving Fraction (SF) of treatment cells.....	92

LIST OF FIGURES

Figure 1. Human skin layers with melanoma that originates from melanocytes.....	3
Figure 2. HPLC standard curve of TMB.....	34
Figure 3. Effect of YSA (YSAYPDSVPMMS) concentration on particle size and zeta potential.....	38
Figure 4. Stability study of TPL.....	40
Figure 5. Effect of trehalose concentration of TPL on zeta potential and particle size after freeze drying.....	43
Figure 6. Solid-state characterization of TPL.....	45
Figure 7. <i>In vitro</i> release study of TPL.....	47
Figure 8. <i>In vitro</i> hemolysis study of TPL at various TMB concentrations.....	49
Figure 9. Uptake study of TPL and YTPL of BRAF ^{V600E} -mutated parent and vemurafenib-resistant melanoma cell lines.....	51
Figure 10. Cytotoxicity assay in melanoma cell lines.....	53
Figure 11. Cytotoxicity assay in parent and vemurafenib-resistant melanoma cell	54
Figure 12. Western blot analysis of EphA2 receptor proteins in A375 and A375R cell lines.....	55
Figure 13. Standard curve of ARV	78
Figure 14. Standard curve of Ni	78
Figure 15. ELISA analysis of TGFβ1 produced by BRAF ^{V600E} mutated melanoma cell lines and its vemurafenib-resistant cell lines.....	80
Figure 16. ARV and Ni synergistically inhibit cell growth in a panel of A375R and SK-MEL-28R.....	82

Figure 17. Cytotoxicity assay in A375R. % Cell viability of A375R after treatment of ARV, Ni and ARNIPL.....	83
Figure 18. ARNIPL characterization.....	85
Figure 19. The stability result of ARNIPL.....	87
Figure 20. <i>In vitro</i> release study of ARNIPL.....	89
Figure 21. Colony forming ability of A375R after treatment with ARV, Ni and ARNIPL	91
Figure 22. Evaluating the effect of ARNIPL on A375R vasculogenic mimicry.....	94
Figure 23. Flow cytometric analysis in A375R.....	96
Figure 24. The effect of various treatments on A375R and A375R+Dermal Fibroblast coculture 3D multicellular tumor spheroids growth.....	100
Figure 25. 3D cell viability assay conducted using CellTiter-Glo® kit.....	103
Figure 26. A375R and coculture 3D spheroids live & dead cell imaging on day 6.....	105

ABBREVIATIONS

UV- Ultraviolet

CSD - Chronic sun-induced damage

NF1- Neurofibromin 1

MAPK - Mitogen-activated protein kinase

MEKi - Mitogen-activated protein kinase inhibitor

BRAFi - BRAF inhibitor

FDA - Food and drug administration

CTLA-4 - Cytotoxic T-lymphocyte-associated protein 4

PD-1 - Programmed cell death protein 1

IFN- α - Interferon-alfa

IL-2 - Interleukin-2

T-VEC: Talimogene laherparepvec

ECM - Extracellular matrix

MMPs - Matrix metalloproteases

BET - Bromodomain and extraterminal domain

PROTAC - Proteolysis-targeting chimeric

CAFs - Cancer-associated fibroblasts

TGF- β - Transforming growth factor- β

FGF - Fibroblast growth factor

HGF - Hepatocyte growth factor

TMB - Trametinib

LVEF - Left ventricular ejection fraction

ILD - Interstitial lung disease

CSR - Central serous retinopathy

AEs - Adverse events

DLS - Dynamic light scattering

DSC - Differential scanning calorimetry

RPM - Rotations per minute

HPLC - High pressure liquid chromatography

PDA - Photodiode-array

CAN - Acetonitrile

ARV- ARV-825

Ni - Nintedanib

ARNIPL - Dual ARV-825 and Nintedanib -loaded PEGylated nanoliposomes

PE - Plating efficiency

SF - Survival fraction

1 Introduction

1.1 Melanoma

Human melanomas are the malignant tumors that develops when melanocytes (pigment-producing cells) begin to grow out of control as shown in Figure 1. Even though melanoma is much less common than basal cell and squamous cell skin cancers, it is more threatening since it's more likely to spread to other parts of the body if not found and treated in the early stage. Melanoma is the fifth most common cancer among men and the sixth most common cancer among women. The approximates of melanoma in the United States is about 100,350 new cases (60,190 men and 40,160 women) to be diagnosed and 6,850 people expected to die of melanoma in 2020 [1]. Melanomas are normally form in the skin though it can also be found in other parts of your body like the eyes, mouth, genitals, and anal area with less chances. Approximately 80% of the melanomas are diagnosed at localized stages and one-third of those early-staged patients tend to develop metastatic melanoma. Even though early detection of melanoma is curable by surgical resection, due to poor prognosis of metastasis, five-year survival rates dropping down from 98% to 17% [2]. There are many risk factors that can enhance the chance of developing melanoma skin cancers. Exposure to ultraviolet (UV) rays either come from too much sun exposure or from man-made sources like indoor tanning beds and sun lamps is the main risk factor of melanoma development. Additionally, other risk factors such as moles, fair skin, weakened immune system, family history of melanoma, and age may also raise the risk of melanoma growth. American Cancer Society suggested three prevention aspects including reducing exposure to UV radiation, watching for abnormal moles, and avoiding weaken immune systems. Cutaneous melanoma on non-

glabrous skin is usually classified into chronic sun-induced damage (CSD melanomas) or those not associated with solar damage (non-CSD melanomas). CSD melanomas normally occurs in in elder individuals and have a high mutation burden related to neurofibromin 1 (NF1), NRAS, BRAF^{nonV600E} or KIT mutations in approximately 20%, while non-CSD melanomas associated with a moderate mutation burden and associated with frequent BRAF^{V600E} mutations and no KIT mutations [3,4]. Clinically, more than 90% of melanomas diagnosed are cutaneous and normally only one mutation can be observed in a patient. Genetic analysis of melanoma has allowed us to identify gene mutation in metastatic melanoma. BRAF mutation is the most frequent genetic abnormalities (approximately 40~60%) among all the mutations in metastatic melanoma and BRAF^{V600E} is the most common mutation (more than 97% of BRAF mutations), where valine is substituted by glutamic acid at codon 600 of the BRAF gene [5,6]. BRAF protein is a serine/threonine protein kinase of 766 amino acids and plays a significant role in mitogen-activated protein kinase (MAPK) pathway, which involved in the transduction of extracellular signals to the nucleus and is important to cell proliferation, differentiation, and survival [7,8].

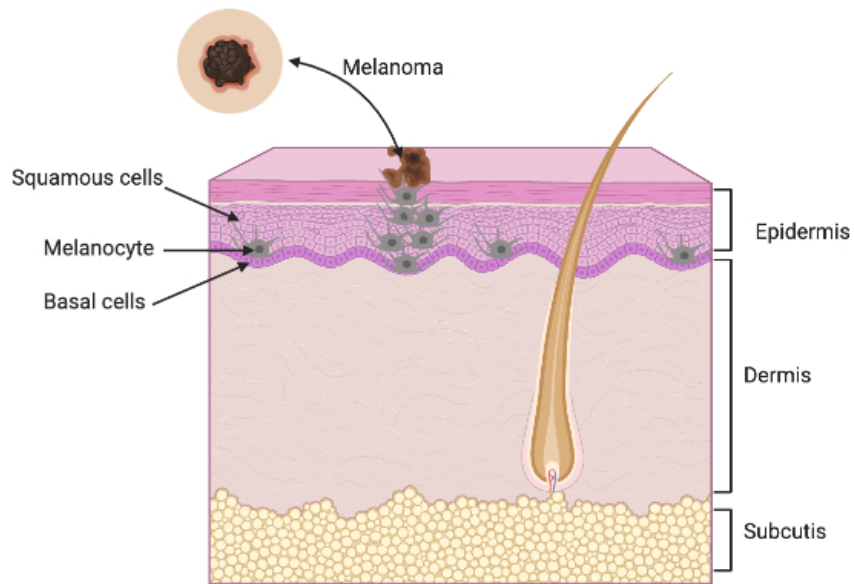


Figure 1. Human skin layers with melanoma that originates from melanocytes.

1.2 Treatment approaches

There are five stages of melanoma depending on the thickness of the tumor and if the melanoma spread or not. Current therapeutic options include surgery, radiation therapy, chemotherapy, immunotherapy, and targeted therapy. The type of treatment(s) depends on many factors, such as the stage and location of the melanoma, patient's overall health, the risk of the cancer returning after treatment, and if the cancer cells have certain gene changes [9,10]. not effective for melanoma since it is normally refractory to conventional chemotherapeutic agents. Dacarbazine was the only FDA approved chemotherapeutic agent for the treatment of metastatic melanoma till 2010. However, dacarbazine has mere 15-20 % overall response rate and was showed enhanced tumor growth and metastasis *in vivo* [11]. Chemo drug is usually not used as the first choice since immunotherapy and targeted drugs have become available. Immunotherapy is designed to stimulate immune system by targeting to checkpoint protein on immune cells, which allows to kill melanoma cells more effectively. The response of immunotherapy depends on the presence of protein on cells. The first agents of FDA-approved immunotherapies in unresectable cutaneous melanomas including anti-PD-1 drugs (nivolumab, pembrolizumab) and anti-CTLA-4 antibody ipilimumab. The FDA approved the immunotherapy combination of ipilimumab and nivolumab for the treatment of unresectable stage III or stage IV melanoma in 2015 and showed increasing response and survival rate. However, it also raises the incidence of adverse effects [12,13] Other therapeutic methods based on immunological response are cytokines (interferon-alfa (IFN- α) and interleukin-2(IL-2)), are used for advanced melanomas in a way that can boost immune system. Adoptive cell therapy or FDA-approved oncolytic viruses

Talimogene laherparepvec (T-VEC) also work as a useful tool in some clinical situations. The side effects of immunotherapy are like fever, achy muscles and joints, fatigue, and nausea. More serious side effects may occur when immune system goes into overdrive and starts to attack healthy tissues. What's more, it also limited by its variable in response and slower onset of action in the clinical use [14,15] . As for targeted therapy, a small portion of melanomas have changes in the C-KIT gene that help them grow. Imatinib (Gleevec) and nilotinib (Tasigna) are targeted drugs that can affect cells with changes in C-KIT. The most frequent mutation in melanoma is BRAF protein and targeting MAPK pathway was found to benefit patients with BRAF^{V600E} mutation [16,17]. The FDA approved targeted drugs that targeting BRAF^{V600E} mutation in MAPK pathway were shown in table 1. Even though targeted therapy provides initial tumor regression, it only offers less than one-year disease control due to the resistance problem [18-20]. Cross resistance to MEK inhibitor was also found in cell lines that acquired BRAF resistance as well as enhanced the toxicity in the combination with BRAF inhibitor, thus limited the long-term survival of patients who harbors BRAF mutations [21-24]. The combination of targeted therapies with immunotherapy has also been explored, nevertheless, the frontline therapy for BRAF-mutant metastatic melanoma is still remaining to be decided due to variable in response, resistant problems as well as some safety concerns [25-27].

Table 1. FDA approved drugs for targeting MAPK pathway of BRAF^{V600E} mutated melanoma. (BRAFi: BRAF inhibitor, MEKi: MEK inhibitor)

Product	Active Ingredient	Approval Date	Mechanism(s)
Zelboraf	Vemurafenib	August, 2011	BRAFi
Mekinist	Trametinib	May, 2013	MEKi
Tafinlar	Dabrafenib	May, 2013	BRAFi
Mekinist + Tafinlar	Trametinib + Dabrafenib	January, 2014	MEKi +BRAFi
Cotellic	Cobimetinib	November, 2015	MEKi
Tafinlar + Mekinist	Dabrafenib + Trametinib	April, 2018	MEKi + BRAFi
Mektovi + Braftovi	Binimetinib + Encorafenib	June, 2018	MEKi + BRAFi

1.3 Tumor stroma in melanoma

Accumulating evidence has shown tumor stromal components play a major role in tumor microenvironment that affect melanoma tumorigenesis, progression and metastasis [28,29]. The tumor stroma mainly composes of extracellular matrix (ECM), immune cells, fibroblasts and signaling molecules. The homeostasis of normal skin melanocytic is dynamically regulated between the melanocytes and their microenvironment, such as keratinocytes, fibroblasts and the extracellular matrix [30]. However, during the development of melanoma from melanocyte, the interaction between neoplastic cells and surrounding stroma is deregulated. Fibroblasts exert a vital function in terms of regulating the homeostasis of ECM since it can secrete proteolytic enzymes that can degrade ECM such as collagenase and matrix metalloproteases (MMPs), as well as collagens and other fibrous macromolecules [31]. Moreover, fibroblasts were involved in the crosstalk between cancer cells and cancer-associated fibroblasts (CAFs), which are the most crucial component in the tumor stroma that associated with tumorigenesis and immune system modulation in a context-dependent manner. The secreted growth factors from tumor cells can initiate the transition of normal fibroblasts to CAFs and CAFs will in turn secrete more growth factors like transforming growth factor- β (TGF- β), fibroblast growth factor (FGF) and hepatocyte growth factor (HGF) and further promote migration and invasion of tumor cells [30,32]. CAFs are a prominent contributor in the desmoplastic tumor stroma and remodel ECM stiffness by crosslinking with collagen network and secreting cytokines to tumor stroma [32,33]. As a result, the stiffness of ECM will promote cell proliferation, increase adherence junction's motility and activate epithelial-mesenchymal transition [34,35]. Furthermore, this dense-than-normal niche isolate tumor

cells from the vessels can severely impede nanomedicine interstitial transport [36]. Therefore, effective cancer therapies could be targeting tumor stroma besides tumor cells, which can reestablish the balance of the ECM.

1.4 Liposomes

The liposomes have been widely studied as nano-vehicle in targeted delivery of chemotherapeutics for cancer treatment and were the first nano-scaled delivery system that translated into clinical use in 1995 [37,38]. Liposomes are lipid-based bilayer vesicles that consist of an aqueous core and can form spontaneously when phospholipids are dispersed in water. This formation is mainly related with hydrophilic and hydrophobic interactions between lipid-lipid and lipid-water molecules, then the lipid molecules will be arranged after the input of energy like sonication and homogenization to achieve a thermodynamic equilibrium and to curve them since the symmetric membranes prefer to be flat (spontaneous curvature $C_0=0$) [39]. This particular structure allows the incorporation of hydrophobic molecules into the bilayer and hydrophilic molecules in the aqueous core. Among the distinct nanoparticulate systems that are investigated to date, liposomal carriers have proven to be advantageous over other types dosage forms due to the function of active and passive targeting that minimize off-target side effects, biocompatibility, enhanced bioavailability, solubility, biodistribution and systemic circulation of antineoplastic agents, which enhance the therapeutic index especially for those multifunctional liposomes with various combination mechanisms [38,40-42]. Because of the unique structure and the phospholipid being a safe and biocompatible excipient, substantiates to be superior when compared to nonionic surfactants and polymers for intravenous delivery.

The mechanism of liposomes for passive tumor accumulation is known as permeability and retention (EPR) effect. This phenomenon is due to the abnormal vasculature that the particle size in the range of 20–200 nm tends to extravasate into the interstitial space.

The particle size out of the range of EPR effect will be either cleared by the kidney or too large to penetrate into the leaky vasculature of tumor tissue [43]. The enhanced retention of nanoparticle is due to the lack of lymphatic drainage. However, the EPR effect is more complicated than previously thought as the extent of EPR effect depends on many factors such as heterogeneity of pathophysiological phenomenon and tumor microenvironment [44].

Further, surface PEGylation of nanoparticle is preferred to bypass the reticuloendothelial system and proteolytic enzymatic degradation [45]. Active targeting liposomes can specific target overexpressed receptor or molecules of the cancer cells by attaching certain moieties on the surface of liposomes, which includes nucleic acids, small molecules, peptides, proteins, carbohydrates, or monoclonal antibodies [46,47].

Nevertheless, pharmaceutical manufacturing, government regulations and intellectual property limited the translation to the clinical application [48,49]. Thus, communication between industry and academia are encouraged to fulfill the potential of liposomal drug delivery systems.

1.5 Literature review

Significant improvement in clinical outcomes with the introduction of targeted therapies based therapeutic regimen has remarkably changed the survival statistics of BRAF-mutated metastatic melanoma in recent years, and MEKi was combined with BRAFi has been shown to improve clinical benefit including progression-free survival, overall survival and response rate [21,22,50]. However, off target toxicities lead to dose interruption, restrict the dose escalation and warrant reduction in the dose of BRAFi and MEKi especially trametinib (TMB). Dose dependents side effects associated with trametinib are: Cardiac, an absolute decrease of >10% in left ventricular ejection fraction (LVEF), ocular and interstitial lung disease (ILD), rash, hypertension, fatigue, peripheral edema, diarrhea and acneiform dermatitis etc [51,52]. Central serous retinopathy (CSR) and hypertension require dose modification. Management of LVEF requires withhold TMB doses for four months or in severe case permanent discontinuation of TMB [52]. The adverse events (AEs) observed in the patients treated with the combination of BRAFi and MEKi are not as common as those treated with chemotherapy and the percentage of patients with AEs is higher than with vemurafenib monotherapy due to the toxicity of MEKi, thus the dose modifications or interruptions are usually required to optimize the use of the treatment base on the effective side-effect management [23]. Therefore, drug delivery to the desired site is preferential for metastatic melanoma tumor cell targeting which prevents unwanted cell destruction.

BRAFi Vemurafenib has been approved by FDA in 2011 for first-line treatment of metastatic melanoma in 2011 due to its promising clinical efficacy [53]. Unfortunately, patients developed vemurafenib-resistance and eventually relapsed over an average of 6

to 8 months [54]. Additionally, cross-resistance of combined BRAF/MEK Inhibition was found in acquired BRAFi resistance [18,20,55]. Various resistant mechanisms have been studied for acquired resistance to BRAFi such as reactivation of the MAPK signaling pathway or PI3K-AKT pathway, upregulation of tyrosine kinase receptor and interactions with the tumor microenvironment [56]. Possible alternative combination therapies and clinical investigations to overcome BRAFi-caused resistance in melanomas with BRAF^{V600E} mutation has been extensively discussed and studied [57,58].

Emerging data has suggested that the pathogenesis of melanoma is due to the aberrant activity of epigenetic regulation of the transcriptional process through the modification of DNA and chromatin, which affected melanoma promotion, metastasis and drug resistance [59,60]. Overexpressed c-MYC was reported to drive melanoma metastasis and major resistance pathways were found to converge to activate c-MYC [61,62]. c-MYC is a major transcriptional factor directly regulated by BRD4 and controls almost all cellular processes. However, the lacking of specific active site makes the direct therapeutic targeting difficult [63]. Indirect targeting to c-Myc by BET bromodomain inhibition was proved as therapeutic strategy in recent years [64-66]. It was also reported that BRD4 is significantly upregulated in primary and metastatic melanoma tissues compared to melanocytes and thus to be considered as a new target for therapeutic strategy [62]. BRD4 is one of the family members of bromodomain and extraterminal domain (BET) proteins, which also contains BRD2, BRD3 and BRDT. BRD4 is an epigenetic reader that regulates gene transcription and cell cycle through recruiting transcriptional regulatory complexes to chromatin [67]. BRD4 contains two N-terminal bromodomains (BD1, BD2) that bind to acetylated lysine residues of histone tails or other nuclear proteins and

influence gene transcription both at initiation and elongation step, as well as affect the expression of oncogenes and anti-apoptotic proteins like Bcl-2 and Bcl-xl [59,68]. Additionally, manipulation BET proteins in melanoma could offset resistance problems and enhanced BRAF/MEK inhibitors efficacy in melanoma [69-71].

PROteolysis-TArgeting Chimeric (PROTAC) technology, using “a kiss of death” to destroy ‘undruggable’ proteins has been discovered in 2001 and was considered as next-generation tool for chromatin regulation [72,73]. The first cereblon-based BRD4 PROTAC molecule ARV-825 was developed by researchers from Yale University and Arvinas, which selectively degrade BRD4 protein by hijacking the E3 ubiquitin ligase cereblon instead of mere inhibiting it, resulting in quick and prolonged degradation of BRD4 compared to traditional small molecule inhibitors [74]. Moreover, ARV-825 was proved to be a novel therapeutic molecule for the treatment of vemurafenib-resistant melanoma [75].

It was reported that melanoma cells can stimulate the recruitment of fibroblasts and activate them, which contributed to melanoma growth as well as drug resistance [76]. Fibroblasts is one of the most predominant cell types that deposit extracellular matrix (ECM), which is associated with all stages of cancer development [30,31]. It was reported that stromal fibroblasts can be activated into cancer-associated fibroblasts (CAFs) since the secretion of growth factors such as transforming growth factor- β (TGF- β) from cancer cells, in turns, CAFs can further stimulate tumorigenesis, migration, invasion and metastasis of cancer cell by secreting more growth factors like TGF- β to the stromal ECM [32]. This crosstalk between cancer cells and CAFs remodel the stromal extracellular matrix (ECM) and contribute to the cancer progression. TGF- β is one of the

major cytokines that derived from CAFs and was found to increases survival of human melanoma through stroma remodeling [33]. BRAF inhibitor vemurafenib treated melanoma cells was found to led TGF- β release, which increased the deposition of fibronectin, type I collagen and α -smooth muscle actin [34,35]. Type I Collagen and hyaluronic acid rich dense extracellular matrix of solid tumor serves as a tortuous, viscous, and steric barrier, which severely restricts the uptake and antitumor efficacy of nanotherapeutics [36].

2 Purpose of Study

The treatment for BRAF-mutant metastatic melanoma has been widely explored aiming to improve the therapeutic benefit, however, the severe toxicity and resistance problems are mainly limited the effectiveness of the therapeutics. Therefore, the purpose of the present research was aiming to address the current problems for BRAF-mutant metastatic melanoma in two perspectives as following:

I) There have been no studies demonstrating EphA2 receptor-targeted nanoparticles with anticancer agents for metastatic melanoma. The first part of the thesis project focus on developing active-targeting nanoliposomes to reduce toxicity of the targeted therapy (TMB) for the treatment of BRAF^{V600E}-mutated melanoma.

Specific Objectives include:

- (1) To develop and characterize YSA-anchored trametinib loaded PEGylated liposomes (YTPL).
- (2) To evaluate anti-melanoma efficacy of YTPL in BRAF^{V600E}-mutated parent cells (lines A375 and SK-MEL-28) and vemurafenib-resistant cells lines (A375R and SK-MEL-28R) in melanoma.

II) The second part of the thesis aim at investigating the effect of BRD4 proteolysis targeting chimera (PROTAC) molecule (ARV-825) and anti-fibrotic agent (Nintedanib) combination and developing a nanoliposomes to resolve the vemurafenib-resistance problem for BRAF^{V600E}-mutated melanoma.

Specific Objectives include:

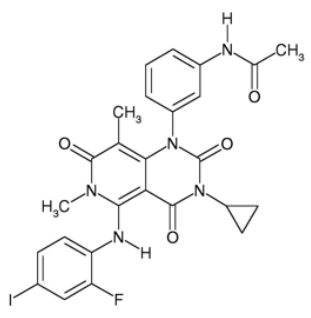
- (1) To evaluate the cytotoxic interaction of BRD4 PROTAC (ARV-825) and anti-fibrotic agent (Nintedanib) in BRAF^{V600E}-mutated vemurafenib-resistant melanoma cells.
- (2) To develop and characterize dual ARV and Nintedanib-loaded PEGylated nanoliposomes (ARNIPL).
- (3) To evaluate anticancer efficacy of ARNIPL in BRAFi resistant human melanoma *in vitro* using vemurafenib-resistant melanoma cell lines.

3 EphA2-Receptor Targeted PEGylated Nanoliposomes for the Treatment of BRAF^{V600E} Mutated Parental and Resistant Melanoma

3.1 Drug (Trametinib)

Trametinib (Mekinist™) is a small molecule that approved as single-agent oral treatment for unresectable or metastatic melanoma in adult patients with BRAF^{V600E/K} mutations by FDA in May 2013, each 1mg tablet contains 1.127 mg trametinib dimethyl sulfoxide equivalent to 1 mg of trametinib non-solvated parent with the recommended dose 2 mg once daily taken at least 1 hour before or at least 2 hours after a meal [77]. Trametinib is a mitogen-activated protein kinase (MAPK) kinase (MEK) inhibitor that can selectively bind to unphosphorylated MEK1 and MEK2 with high affinity and allosterically inhibits their kinase activity, thus suppress the growth factor-mediated cell signaling pathway that involve in cell proliferation, survival and differentiation [77-79]. The properties of Trametinib was shown in Table 2. Trametinib was combined with BRAF inhibitor dabrafenib in order to delay the resistance to BRAF inhibition [80]. FDA approved the combination of trametinib with dabrafenib on January,2014 for the treatment of BRAF^{V600E/K} mutant metastatic melanoma and on May, 2018 as an adjuvant treatment for BRAF^{V600E} mutated, stage III melanoma after surgical resection based on the results of the COMBI-AD phase 3 study [81,82].

Table 2. Trametinib drug profile

Name	Trametinib
Chemical Name	N-[3-[3-cyclopropyl-5-(2-fluoro-4-iodoanilino)-6,8-dimethyl-2,4,7-trioxypyrido[4,3-d]pyrimidin-1-yl]phenyl]acetamide
Molecular formula	C ₂₆ H ₂₃ FIN ₅ O ₄
Molecular weight	615.39 g/mol
Structure	 <p>The chemical structure of Trametinib is a complex heterocyclic molecule. It features a central pyrido[4,3-d]pyrimidin-1,2,4,7-tetrone core. This core is substituted with a methyl group (CH₃) at the 6-position, a methylamino group (NHCH₃) at the 8-position, and a cyclopropylamino group (NH-cyclopropyl) at the 2-position. The 3-position of the pyrimidine ring is linked to a phenyl ring, which is further substituted with an acetamido group (NHCOCH₃) at the para position. The 5-position of the pyrimidine ring is linked to another phenyl ring, which is substituted with a fluorine atom (F) at the 2-position and an iodine atom (I) at the 4-position.</p>
CAS No.	871700-17-3
Melting point	299°C-301°C
LogP	1.965
Solubility	DMSO 32 mg/mL, Water <1.2mg/mL, Ethanol <1.2mg/mL
BCS class	Class II

3.2 Erythropoietin-producing hepatocellular (EphA2) receptor

EphA2 is a protein tyrosine kinase receptor that belongs to Eph family and it binds to ephrin-A ligands through glycosphosphatidylinositol linkage [83]. Normally, EphA2 is expressed in the epithelial and endothelial cells while it has been found to be as a promoter of melanoma tumorigenicity [84]. Recent studies demonstrated the pivotal role of overexpressed EphA2 receptors in aggressiveness, metastatic potential, and vasculogenic mimicry in malignant melanoma [84,85]. EphA2 is also considered a growth receptor for malignant melanoma [86]. Melanoma tumor samples from patients taken prior to or after treatment with BRAFi and MEKi showed very high expression of EphA2 in both BRAF^{V600E} and BRAF^{WT} melanomas. Compared to the EphA2 expression in malignant melanoma, normal tissues have low EphA2 expression, and therefore using YSA peptide-anchored nanocarriers for drug delivery may reduce off target side effects by reducing exposure of cytotoxic drugs to normal cells [87]. Moreover, upregulation of the EphA2 receptor was observed in BRAFi-resistant cell lines (such as A375 and SK-MEL-28) [88]. Thus, the cell surface EphA2 receptor could be a potential target not only for treatment but also for delivering a high payload of anti-melanoma drugs. Wu et al. demonstrated that YSA-conjugated paclitaxel was more effective in murine melanoma compared to paclitaxel alone [89]. Moreover, YSA-anchored nanocarriers can carry a much higher load of a drug to the tumor compared to individually conjugated molecules [90].

3.3 Materials

Trametinib was purchased from LC Laboratories (Woburn, MA, USA); 1,2-Dioleoyl-sn-glycero-3-phosphocholine (DOPC) was purchased from Cordenpharma (Liestal, Switzerland); PE 18:0/18:0-PEG2000 was obtained from Lipoid (Ludwigshafen, Germany); cholesterol, chloroform, and a Sephadex G50 column were purchased from Sigma-Aldrich (St. Louis, MO, USA); 6-histidine tagged PEGylated (PEG) YSA (6His-PEG-YSA) was obtained from GenScript Corporation (Piscataway, NJ, USA); (1,2-dioleoyl-sn-glycero-3-[N-(5-amino-1-carboxypentyl)-iminodiacetic acid] succinyl (nickel salt) (DOGS-NTA-Ni)) was obtained from Avanti (Alabaster, AL, USA); Fetal Bovine Serum (FBS) was procured from Atlanta Biologics (Oakwood, GA, USA); Dulbecco's modified Eagle's medium (DMEM) and the BCA protein estimation kit were purchased from ThermoFisher Scientific Inc. (Waltham, MA, USA); Penicillin–Streptomycin–Amphotericin B (PSA) was purchased from MP Biomedicals, LLC (Solon, OH, USA); and ALW-II-41-27 was obtained from Cayman Chemical (Ann Arbor, MI, USA). Other chemicals and solvents were of analytical grade. Melanoma cell lines (A375 and SK-MEL-28) were obtained from American Type Culture Collection (Manassas, VA, USA).

3.4 Methods

3.4.1 Analytical Method

Chromatographic separation of TMB was achieved using Waters e2695 separation module, a 2998 PDA detector instrument equipped with a Hypersil ODS C18 column (250mm×4.6mm,5µm). Acetonitrile: phosphate buffer pH 3.5 (70:30) was used as the mobile phase with a flow rate of 1 mL/min and an injection volume of 10 µL. The column temperature was kept at 25 °C and the output signal was detected using Empower 3 software. The retention time of TMB was found to be 4.7 min, detected at 248 nm. All measurements were made in triplicate (n=3).

3.4.2 Cell Culture

Vemurafenib-resistant cell lines (A375R and SK-MEL-28R) were generated by adding 0.2 μ M of vemurafenib to the media of A375 and SK-MEL-28 for 2 months. The vemurafenib resistance was confirmed prior to studies. All cell lines were maintained in DMEM, supplemented with 10% FBS and 1% PSA, and incubated at 37 °C with 5% CO₂.

3.4.3 Preparation of Liposomes

Initially, liposomes were prepared by modified hydration methods. Briefly, TMB: DOGS-NTA-Ni: DOPC: cholesterol: DSPE-PEG 2000 in a 1:0.75:60:16.3:2.1 molar ratio was dissolved in chloroform. DOPC, cholesterol, DSPE-PEG, and TMB were dissolved in chloroform. For thin film hydration, the solution was taken in a round bottom flask under vacuum to form a film, followed by hydration with water at 55 °C and ultrasonication (30% amplitude) for 2 min. For the modified hydration method, the same chloroform solution was added dropwise to parenteral-grade mannitol (200 µm) with constant stirring at 45 °C and left overnight for evaporation of chloroform. Dispersion of this resultant powder was prepared in water at 55 °C and was sonicated (30% amplitude) for 2 min. For the investigation of the effect of mannitol on stability, mannitol was separated from liposomes using a Sephadex G50 column. For preparation of YTPL, first DOGS-NTA-Ni-loaded liposomes were prepared using the same composition and method described above. Liposomes were incubated with different concentrations of YSA for 30 min to obtain liposomes with varied molar ratios of DOGS-NTA-Ni: YSA.

3.4.4 Characterization of liposomes

The average size, size distribution by intensity, zeta potential, and polydispersity index were measured using a dynamic light scattering (DLS) particle size analyzer (Malvern Zetasizer Nano ZS, Royston, UK). Samples were analyzed using disposable cuvettes at 25 °C with a scattering angle of 173°. The effect of YSA concentration on particle size and zeta potential was evaluated. All the experiments were carried out in triplicates. Entrapment efficiency was estimated using ultrafiltration by Amicon ultra centrifugal filters (50K). The concentration of TMB was analyzed by HPLC. The encapsulation efficiency of TMB was expressed as the percent of drug encapsulated and calculated using the following formula:

$$\text{Percent encapsulated} = ((\text{Total TMB}) - (\text{Free TMB})) / (\text{Total TMB}) \times 100\%.$$

3.4.5 Stability Study

TPL at different drug loading values (1%, 2.5%, and 4%) was prepared for the stability study. Total drug content was measured at time zero. Samples were withdrawn at different time points to analyze the amount of precipitated drug by HPLC.

3.4.6 Freeze Drying of Liposomes

TPL with 1% drug loading was used to investigate the effect of concentration of cryoprotectant (2.5%, 5%, 7.5%, 10% trehalose) on freeze drying. TPL was prepared using the method described above (unfiltered TPL). Further, unfiltered TPL was passed through a Sephadex G50 gel column to separate mannitol. Mannitol-free TPL was referred to as filtered TPL. Briefly, 1-mL aliquots of the liposomal dispersions were filled into colorless glass vials and then stored at -80 °C overnight, followed by lyophilization (Labconco FreeZone 2.5, -53 °C at 12 Pa) overnight in order to achieve a preservable white powder. The same protocol was used for freeze drying of YTPL. Lyophilized liposomes were reconstituted with water. Particle size, zeta potential, and YSA binding efficiency were analyzed before and after freeze drying of YTPL. For YSA binding efficiency, 400 μ L of YTPL were filled into Amicon Ultra centrifugal filters (30 kDa) (Millipore, Ireland). Free YSA was separated by centrifuging the samples at 10,000 rpm for 10 min. Concentration of free YSA (before and after freeze drying) was analyzed using a BCA protein estimation kit (Thermoscientific, Waltham, MA, USA). Briefly, 400 μ L of YSA coated liposomes was filled into Amicon Ultra centrifugal filters (30 kDa) (Millipore, Ireland) and free YSA was separated by centrifuging the samples at 10,000 rpm for 10 min. Concentration of free YSA (before and after freeze drying) was analyzed using a BCA protein estimation kit.

3.4.7 Differential Scanning Calorimetry (DSC) Thermograms of TMB and TPL

Analysis of TMB and TPL was carried out to evaluate the physical state of TMB in liposomes using a Q200 modulated DSC instrument (TA Instruments, New Castle, DE, USA). The liposomal formulation was dried, and the semi-solid paste was weighed in an aluminum pan and hermetically sealed. The samples were equilibrated at 25 °C for 5 min and were heated at the rate of 10 °C/min from 40 °C to 350 °C. A hermetically sealed empty aluminum pan was used as a reference. TA Instruments Universal Analysis 2000 software (TA Instruments) was used to analyze the data.

3.4.8 *In Vitro* Release Study

Drug release from TPL was carried out using the dialysis bag method. Before use, dialysis bags (Spectra/Por® 7) were soaked before use in Milli-Q water at room temperature overnight to remove the preservative, followed by rinsing thoroughly in Milli-Q water. Drug release of TMB from TPL was carried out in a dialysis sac with 200 mL of phosphate buffer saline (pH 7.4) containing 0.5% Kolliphor EL at 37 °C with constant stirring. The samples were withdrawn from the release medium at different time intervals. The amount of TMB in the release media was evaluated by HPLC.

3.4.9 *In Vitro* Hemolysis Study

Rat red blood cells (RBCs) were separated from plasma by centrifugation at 2000 rpm for 5 min. The cell pellet was re-dispersed into an appropriate volume of PBS to achieve the same hematocrit. Then, 1 mg/mL TMB of TPL was added to the RBC dispersion to achieve 100, 50, 10, and 2 µg/mL TMB concentrations. After 30 min of incubation at 37 °C, samples were centrifuged at 2000 rpm for 10 min. Supernatants were diluted with PBS and analyzed. A UV spectrophotometer was used to evaluate the hemoglobin release at 550 nm. PBS was used as the negative control, and sodium lauryl sulfate solution was used as the positive control (100% hemoglobin release). Percentage hemolysis was calculated by following formula:

$$\% \text{ hemolysis} = (\text{absorbance of test sample} - \text{absorbance of negative control}) / (\text{absorbance of positive control} - \text{absorbance of negative control}) \times 100$$

3.4.10 Plasma-to-Blood Ratio

TPL was added to blood to prepare TMB at a concentration of 50 $\mu\text{g/mL}$ ($n = 6$). Samples were incubated at 37 $^{\circ}\text{C}$ for 30 min and then samples were centrifuged. Plasma was separated from centrifuged samples. Sodium lauryl sulfate was added to half the samples for complete hemolysis. The TMB concentration in hemolyzed blood and plasma was analyzed by HPLC. The plasma-to blood ratio was calculated by the equation given below:

$\text{CB/CP} = \text{Concentration of TMB in whole blood/Concentration of TMB in plasma}$

3.4.11 Cellular Uptake of Liposomes

Cells were plated in a 96-well plate at a density of 10,000 cells/well and incubated at 37 °C and 5% CO₂ for 48 h before treatment. Coumarin-6 loaded PEGylated liposomes (TPL) and YSA-anchored coumarin-6-loaded PEGylated liposomes (YTPL) were incubated with cells for 1 h. Afterwards, cells were washed with HBSS and fixed with 3.7% formalin. Uptake of TPL and YTPL in different cell lines was observed for same exposure time using the EVOS FL Auto Cell Imaging System with 40 × magnification.

3.4.12 *In Vitro* Cytotoxicity Test

SK-MEL-28R cell lines using 3-(4,5-dimethylthiazol-2-yl)-2,5-diphenyl tetrazolium bromide (MTT) assay. ALW-II-41-27 (an EphA2 receptor ATP-competitive inhibitor), vemurafenib, and vemurafenib with 0.1 μ M ALW-II-41-27 were tested in both SK-MEL-28 and SK-MEL-28R. Cells were seeded in 96-well plates at a density of 5000 cells/well and allowed to grow for 24 h before treatments. TMB and TPL were diluted in cell culture medium at different concentrations. After 48 h treatment, cell viability was determined by the MTT assay. Briefly, MTT dye was dissolved at a final concentration of 5 mg/mL in PBS. Cells were incubated with 20 μ L of 5 mg/mL MTT solution in each well for 3 h at 37 °C, 5% CO₂. Then the medium was removed from wells and MTT-formazan crystals were dissolved by the addition of 100 μ L of dimethyl sulfoxide (DMSO) to each well. The quantity of MTT-formazan was determined by 570 nm absorbance as the wavelength reference.

3.4.13 Western Blot Assay

Whole cell protein lysates were obtained from A375, SK-MEL-28, A375R, and SK-MEL-28R cell lines. Briefly, cells were scraped in modified RIPA buffer (50 mM Tris, 150 mM NaCl, 1% v/v NP-40, 0.5% w/v deoxycholate, 0.1% w/v SDS, 10% v/v glycerol, 10 mM NaF, 0.4 mM EDTA, pH 8.0) with protease inhibitors. The lysates were cleared by centrifugation at 10,000 g for 10 min and then reduced with Laemmli buffer containing β -mercaptoethanol, separated on 4–15% MiniProtean TGX gels (Bio-Rad, Deesid, UK), transferred to a PVDF membrane, and probed with primary antibodies from Cell Signaling Technology for EphA2 (6997) and β -actin (8457) for chemiluminescence detection using the Azure Biosystems c500 imager (Dublin, CA, USA).

3.4 Results and Discussion

3.4.1 Analytical Method

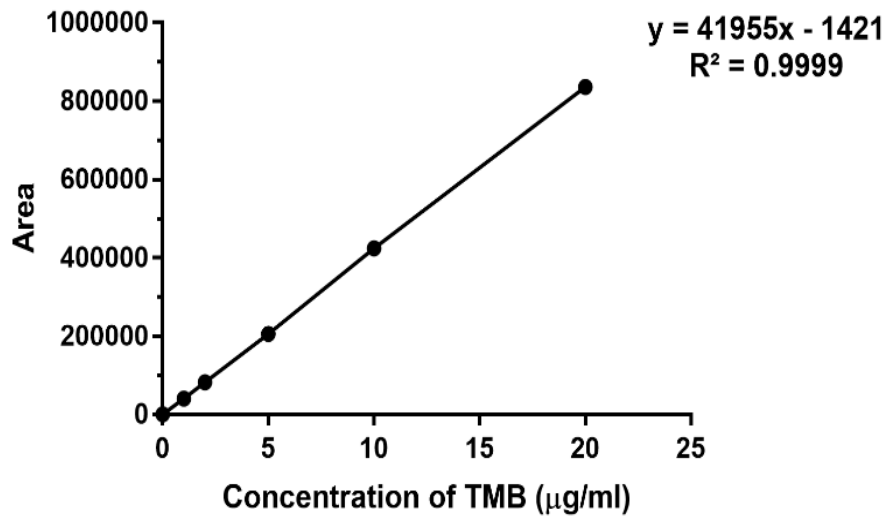


Figure 2. HPLC standard curve of TMB.

3.4.2 Preparation of TMB-Loaded PEGylated Liposomes

Since there are no previous reports on formulation development of TMB, we explored four different methods for preparation of TPL, which were compared and optimized based on formulation feasibility and physical stability. The results of TPL prepared using different methods are given in Table 3. Due to the poor solubility of TMB in ethanol and ether, the ethanol injection method and ether injection method were not used for the preparation of TMB liposomes. The thin film hydration method is a commonly used method for the preparation of liposomes. However, around 50% of the drug precipitated from TPL in 2 h. Moreover, entrapment efficiency was only 51.6%. Because of the poor entrapment and physical stability of TPL prepared using a thin film hydration method, we adopted a modified hydration method, which showed 96.2% entrapment of TMB and better physical stability (absence of TMB precipitation within 24 h) compared to the thin film hydration method. Thus, a modified hydration method was used for further development of YSA-anchored trametinib-loaded PEGylated nanoliposomes (YTPL).

Table 3. Methods for the preparation of trametinib (TMB)-loaded PEGylated liposomes (TPL).

Method	Solubility of TMB	Entrapment Efficiency of TPL (1% w/w TMB loading)
Thin film hydration	Soluble	51.6%
Modified hydration	Soluble	96.2%

3.4.3 Particle Size and Zeta Potential

Particle size and zeta potential of nanoparticles play an important role, especially for parenteral administration. Different concentrations of 6His-PEG-YSA peptides were used to optimize particle size and zeta potential. The succinyl group of DOGS-NTA-Ni contributes to negative zeta potential of the liposomes. The hydrodynamic diameter of TPL prepared using a modified hydration method was found to be 109.45 ± 9.40 nm with a zeta potential of -35.55 ± 9.60 mV. The zeta potential of DOGS-NTA-Ni-loaded liposomes was lower than TPL. For YTPL, particle size was found to be similar at all the DOGS-NTA-Ni:YSA ratios (Figure 3). A slight decline in particle size from 109.45 nm to 89.75 nm was observed after incubation with YSA. An increase in the zeta potential of liposomes was observed in a concentration-dependent manner due to the surface complexation of YSA (Figure 1b). Since electropositive transition metals Ni showed high affinity to bond with side chain of Histidine, imidazole. Therefore, Nickel-chelating lipids DOGS-NTA-Ni can bind with hexahistidine chain of YSA peptide, and allow one simple step of YSA to attach on the surface of the liposomes. Due to the complexation between the YSA target ligand and DOGS-NTA-Ni, the zeta potential changed from negative to positive in a YSA concentration-dependent manner. The zeta potential significantly increased from -28.10 mV to -0.92 mV upon addition of 1:1.25M DOGS-NTA-Ni: YSA. Thereafter, there was only a slight increase in zeta potential at higher ratios (e.g., 1:2.5 and 1:5), suggesting that YTPL was saturated with YSA. Thus, a 1:2.5 molar ratio of DOGS-NTA-Ni:YSA was used as an optimized ratio for YTPL.

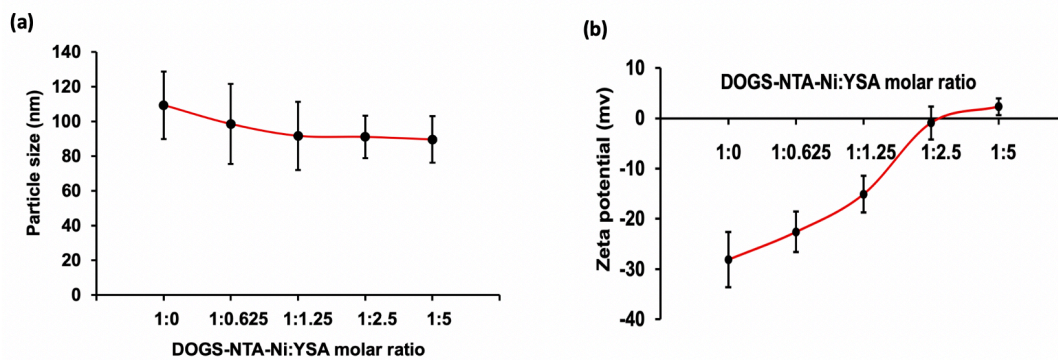


Figure 3. Effect of YSA (YSAYPDSVPMMS) concentration on (a) particle size and (b) zeta potential. Data are given as mean \pm SD ($n = 3$). No significant change in particle size while zeta potential increased as YSA concentration increased.

3.4.4 Stability of Liposomes

The precipitation of a hydrophobic drug from liposomes is another issue with respect to long term stability. In order to evaluate the physical stability, TPL with different drug loading values (1%, 2.5% and 4%) at a 0.5 mg/mL TMB concentration were prepared. As expected, we observed that lower the drug loading, the lower the percentage of TMB precipitation (Figure 4). Moreover, the precipitation increased with time. For TPL with 4% drug loading, more than 25% of the drug precipitated within half an hour, while at 2.5% drug loading of TPL, the precipitation was slower compared to 4%. However, more than 14% of the drug precipitated in 1 h. An increase in percentage precipitation with time suggested that TPL in liquid form may not be stable for long periods. Thus, considering the poor physical stability of TPL in liquid form, freeze drying was carried out. TPL with 1% loading was considered for freeze drying. Moreover, we investigated the effect of storage conditions (room temperature and 4 °C) on liposome stability. For 4% and 2.5% drug loading, precipitation was significantly affected by storage conditions. For 1% drug loading, precipitation was less than 5% at room temperature and 4 °C in 24 h (Data not shown). Nevertheless, we observed a very slow but steady increase in drug precipitation from liposomal formulation over the time period. Thus, it was essential to convert the liposomal formulation into powder for reconstitution.

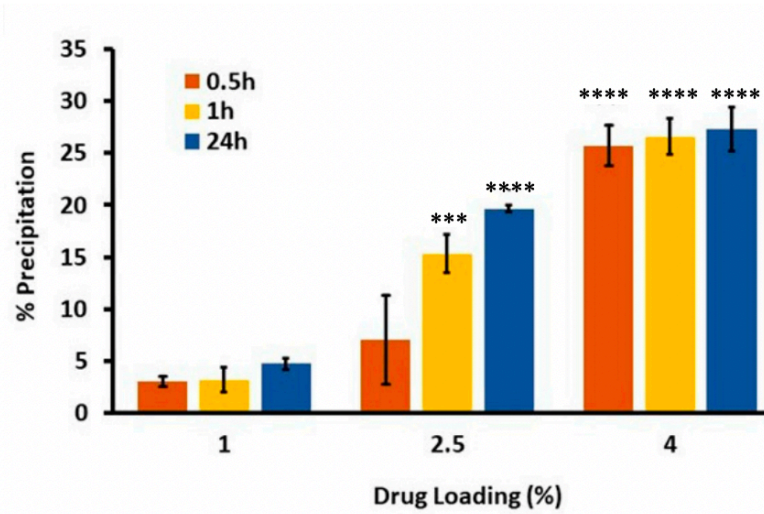


Figure 4. Stability study of TPL. % precipitation of TPL with varying drug loading values. Precipitation significantly increased with higher drug loading compared to 1% drug loading. * $p < 0.05$ and ** $p < 0.01$. Data are given as mean \pm SD (n = 3).

3.4.5 Freeze Drying of Liposomes

For liposomes with poor physicochemical stability, spray drying or freeze drying are used to address the stability problem. Freeze drying, also known as lyophilization, is the most commonly used method to dry liposomal dispersions. This technique is widely used for pharmaceuticals to improve their long-term storage stability [91]. AmBisome® and Visudyne® are available as lyophilized liposomal powders [92]. Trehalose is one of the most widely used cryoprotectant and it usually exerts the best protective effect among the disaccharides. Trehalose-based products such as Avastin®, and Lucentis® are commercially available. Trehalose has an ability to reduce hygroscopicity so that hydrogen bonds can form easily, has low chemical reactivity, and has a high glass transition temperature (T_g) [93]. Mannitol was used as a carrier for the liposomes and it is generally not advised for stabilizing liposomes because it may separate from a frozen solution or crystallize within the lyophilized cakes [94,95].

Freeze drying was carried out to convert TPL into solid powder for reconstitution. Since TPL was prepared using a modified hydration method that contains mannitol, we evaluated the effect of mannitol on TPL stability. Unfiltered TPL are liposomes without the separation of mannitol. Filtered TPL was prepared by separating mannitol using a G50-Sephadex column while the unfiltered TPL was the liposome which had not undergone filtering of the mannitol. Particle size and zeta potential of unfiltered and filtered TPL before and after freeze drying with various concentrations of trehalose are depicted in Figure 5. We observed that concentration of trehalose plays a significant role in the particle size of reconstituted TPL. Batches with 5% and 7.5% of trehalose

exhibited a paste-like appearance with poor flow properties and took a longer time for reconstitution. TPL with 10% trehalose gave free flow powder and could be reconstituted within 5 min with the original particle size and zeta potential. For TPL with 2.5% trehalose, reconstitution could not be achieved. Therefore, 10% trehalose was used for freeze drying of optimized YTPL. Freeze-dried liposome contains 2.83 μg TMB/mg of powder. No significant change of zeta potential was observed, as shown in Table 4. Particle size was increased but was still within 200 nm. Moreover, the encapsulation efficiency of YTPL remains the same (>96%) as before freeze drying. No significant different of YSA binding percentage was observed before and after freeze drying (more than >95% YSA binding on the liposomes), which is complementary to the result of zeta potential.

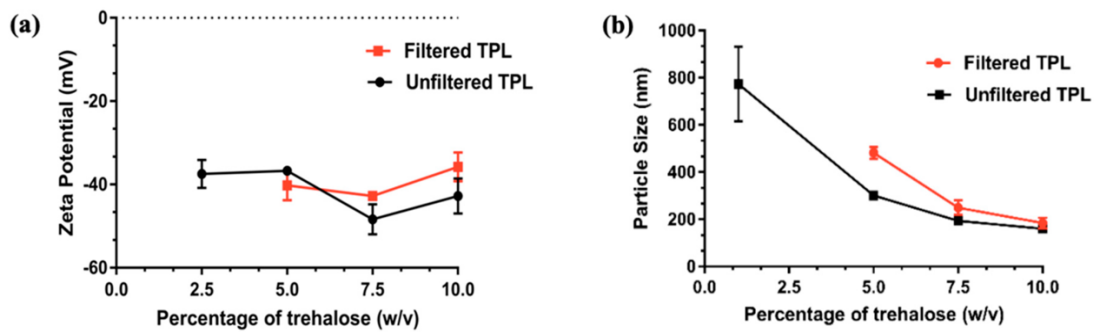


Figure 5. Effect of trehalose concentration of TPL on (a) Zeta potential (b) Particle size after freeze drying. Trehalose concentration has a major effect on particle size and a minor effect on zeta potential. Data are given as mean \pm SD (n = 3).

Table 4. Particle size and zeta potential of YSA-anchored TMB-loaded nanoliposomes (YTPL) and TMB-loaded nanoliposomes (TPL) after freeze drying.

	Particle Size (nm)		Zeta Potential (mV)	
	Before Freeze Drying	After Freeze Drying	Before Freeze Drying	After Freeze Drying
YTPL (10% trehalose)	91.20 \pm 12.16	159.10 \pm 7.50	-0.92 \pm 3.27	-4.44 \pm 0.49
Unfiltered TPL	109.45 \pm 9.40	128.40 \pm 1.84	-35.55 \pm 9.60	-47.30 \pm 1.61

3.4.6 DSC Thermograms of TMB and TPL

Differential scanning calorimetry (DSC) studies can be used for liposome quality control by thermal analysis to determine purity, polymorphic forms, and the melting point of the sample [96]. DSC endotherms of TMB and TPL were obtained as shown in Figure 6. TMB showed a sharp endothermic peak of pure TMB at 300 °C, which suggests that the pure TMB was in a crystalline form. As expected, liposomes did not show any melting endothermic peak. Therefore, the absence of a sharp endothermic peak at 300 °C in liposomes confirmed that TMB was not in a crystalline or precipitated state but was in a solubilized state within lipid bilayers.

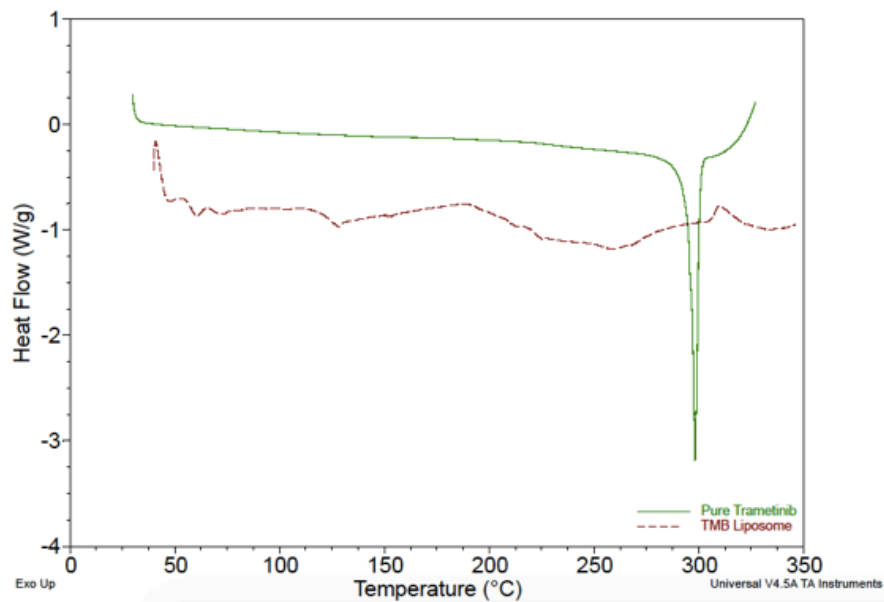


Figure 6. Solid-state characterization of TPL. Differential scanning calorimetry (DSC) thermograms of TMB and TPL. Green peak showed a crystalline form of TMB; the absent peak of the red line showed TMB was in soluble state in liposome.

3.4.7 Drug Release Study

The release of liposomes is important to evaluate the quality of the formulation as well as to predict *in vivo* behaviour of a liposomal drug delivery system. In this study, TPL showed less than an 8% drug release in 24 h at sink conditions (Figure 7), which indicated that TPL did not leak or have burst release of TMB from the liposomes. We anticipate that TPL will follow a similar release behavior *in vivo*. TMB will be confined within the liposome and will not show any burst release in the blood. However, it showed promising activity in our *in vitro* studies, indicating that TMB will be released and act after internalization by cancer cells. We expect liposomes to accumulate at tumor site due to the EPR effect, and for complete release of TMB at the tumor site *in vivo* due to the active-target effect. Sink condition was maintained by adding a non-ionic surfactant Kolliphor EL in the release medium.

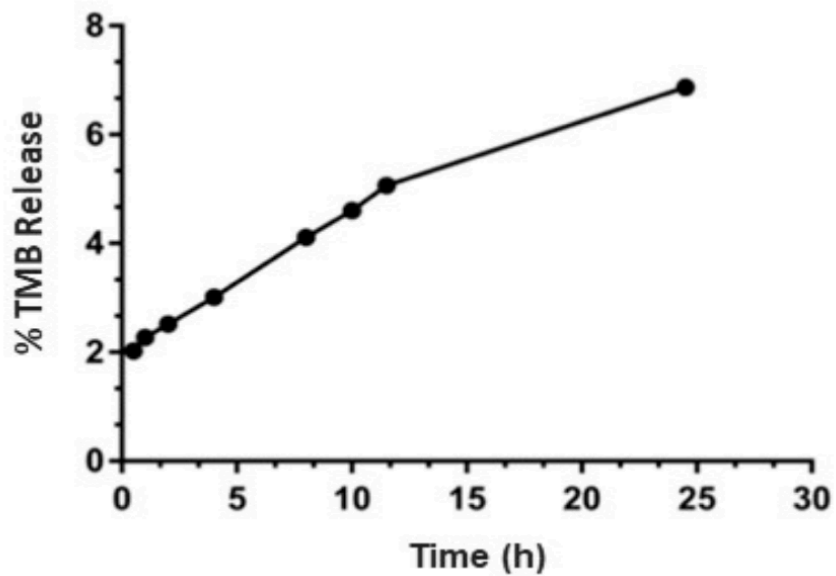


Figure 7. *In vitro* release study of TPL. No hemolysis was observed. Limited amount of release in pH 7.4 at sink condition. Data are expressed as mean and standard deviation.

3.4.8 *In Vitro* Hemolysis Study and Plasma to Blood Ratio

Negligible hemolysis was observed even at 100 µg/mL of TMB used (Figure 8, Table 5). Further, very quick and complete redispersion of red blood cells (RBCs) implied that the surface characteristics of RBCs were not altered by TPL. The blood-to-plasma ratio determines the concentration of the drug in the general circulation and the concentration of the target drug in plasma, which provides an indication of drug the binding to erythrocytes. The result for blood-to-plasma ratios of TMB is around 1 which indicates that TMB is evenly distributed in plasma and red blood cells.

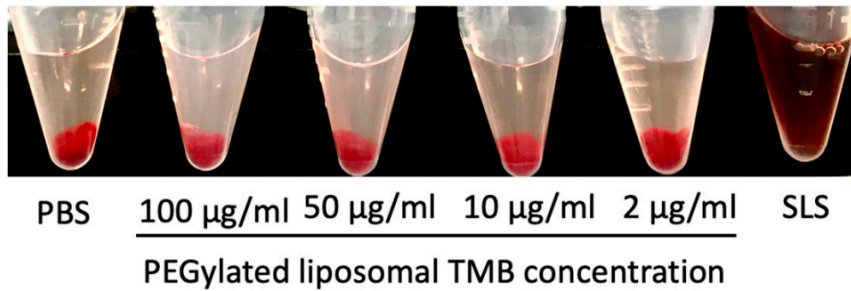


Figure 8. *In vitro* hemolysis study of TPL at various TMB concentrations.

Table 5. *In vitro* hemolysis study of TPL at various TMB concentrations.

	TMB Concentration (µg/mL)			
	100	50	10	2
% Hemolysis	5.14	3.70	1.03	0

3.4.9 Uptake Study

Coumarin-6 was selected as the fluorescent dye for labelling the liposomes. The intensity of this fluorescence dye can be correlated with the extent of liposome uptake. As shown in Figure 9, the intensity of green fluorescence was significantly higher in YTPL-treated cells compared to TPL-treated cells due to the targeting peptide. Moreover, A375 and SK-MEL-28 cell lines showed higher intracellular fluorescence intensity than A375R and SK-MEL-28R for YTPL due to the higher expression of EphA2 receptors, which indicated that the expression of EphA2receptor could be lower in vemurafenib resistant cell lines.

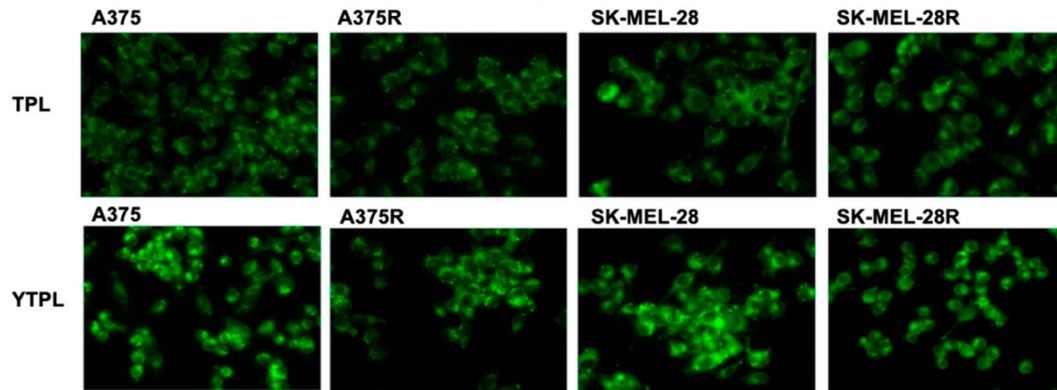


Figure 9. Uptake study of TPL and YTPL of BRAF^{V600E} mutated parent and vemurafenib-resistant melanoma cell lines. High intensity of fluorescence was observed with targeted liposome treatment and resistant cell lines showed less uptake of liposomes. Images were captured at 20× magnification.

3.4.10 *In Vitro* Cytotoxicity Test

In vitro cytotoxicity of TMB, TPL, and YTPL was evaluated in patent cell lines only. IC₅₀ values of each of the formulations is given in Table 6. The IC₅₀ values for TMB, TPL, and YTPL were similar at around 0.7 nM. Cell viability graphs of TMB, TPL, and YTPL in melanoma cell lines are given in Figure 10. The very low IC₅₀ of the TMB liposome confirmed that TMB was released after internalization of TPL into cancer cells. Moreover, the IC₅₀ values of TMB, TPL, and YSL are similar in A375 and SK-MEL-28, while in-vivo behavior may vary due to drug distribution and the microenvironment of the tumor.

To further investigate whether the EphA2 receptor was correlated with vemurafenib-resistance, ALW-II-41-27, an EphA2 ATP-competitive inhibitor, inhibited the growth of SK-MEL-28 and SK-MEL-28R in a concentration-dependent manner (Figure 11). The IC₅₀ values of ALW-II-41-27 were 122.4 nM and 177.0 nM for SK-MEL-28 and SK-MEL-28R, respectively. Co-treatment with ALW-II-41-27 did not alter the cytotoxicity of vemurafenib in parent or vemurafenib-resistant SK-MEL-28 cells. Vemurafenib diluted in 0.1 μM ALW-II-41-27 showed similar viability compared to single vemurafenib treatment, which indicates that the EphA2 inhibitor did not change the resistance sensitivity. Thus, EphA2 receptor inhibition is not co-related to cytotoxicity of vemurafenib or vemurafenib resistance in melanoma.

Table 6. *In vitro* cytotoxicity of TMB, TPL, and YTPL in A375 and SK-MEL-28.

IC ₅₀ (nM)	A375	SK-MEL-28
TMB	0.83 ± 0.36	0.74 ± 0.38
TPL	0.68 ± 0.15	0.60 ± 0.13
YTPL	0.69 ± 0.40	0.77 ± 0.15

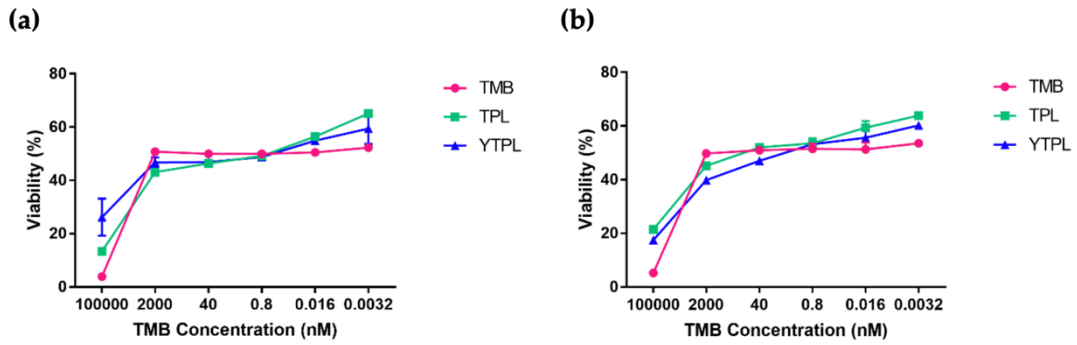


Figure 10. Cytotoxicity assay in melanoma cell lines. % Cell viability of (a) A375 cells and (b) SKMEL-28 cells after treatment of TMB, (TMB loaded PEGylated Liposomes) TPL and YTPL (YSA anchored TPL).

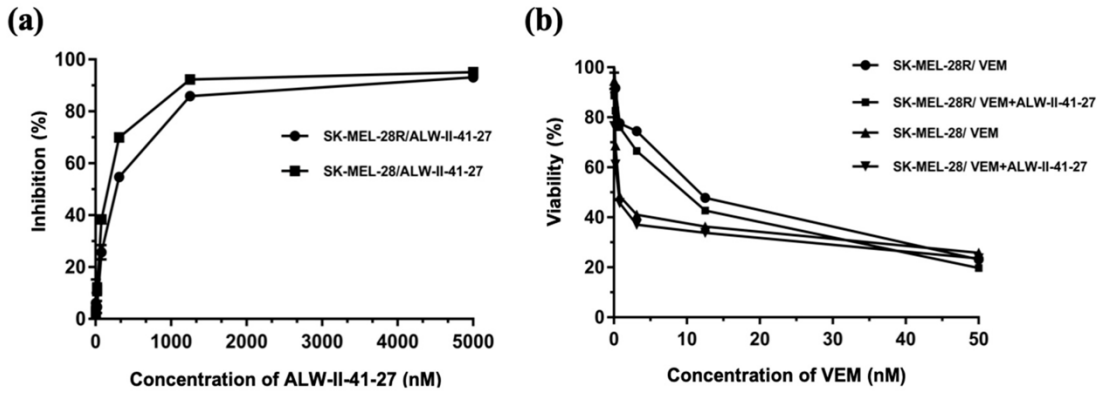


Figure 11. Cytotoxicity assay in parent and vemurafenib-resistant melanoma cell lines (a) % Cell growth inhibition of SK-MEL-28 and SK-MEL-28R after ALW-II-41-27 treatment (b) % Cell viability of SK-MEL-28 and SK-MEL-28R after vemurafenib treatment with and without ALW-II-41-27. Vemurafenib was incubated with 0.1 μ M ALW-II-41-27. Results showed no difference in viability compared to a single vemurafenib treatment alone.

3.4.11 Western Analysis

The protein expression of EphA2 was significantly lower in the whole cell lysates from A375R and Sk-MEL-28R melanoma cell lines compared to A375 and Sk-MEL-28 (Figure 12). The results further confirm that the expression of EphA2 receptor is higher in BRAF^{V600E}-mutated melanoma parent cell lines compared to the resistant cell lines.

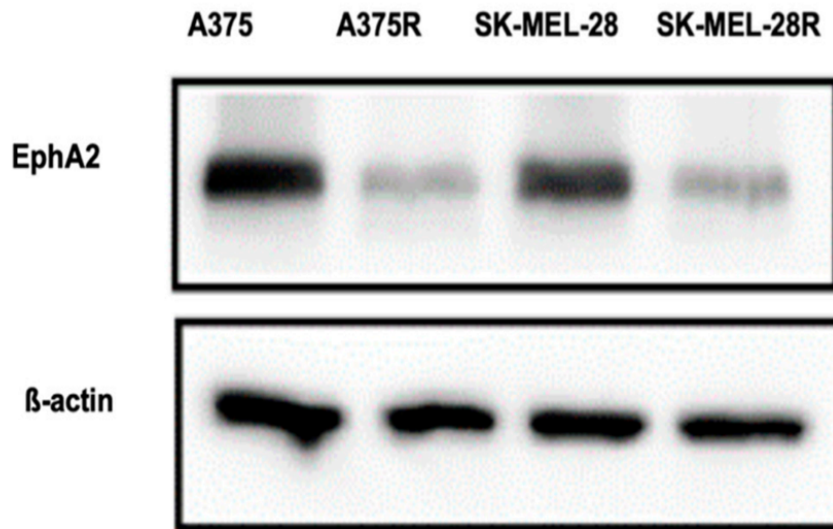


Figure 12. Western blot analysis of EphA2 receptor proteins in A375 and A375R cell lines. Higher EphA2 receptor expression was observed in BRAF^{V600E}-mutated cell lines than in the vemurafenib-resistant cell line (n = 3).

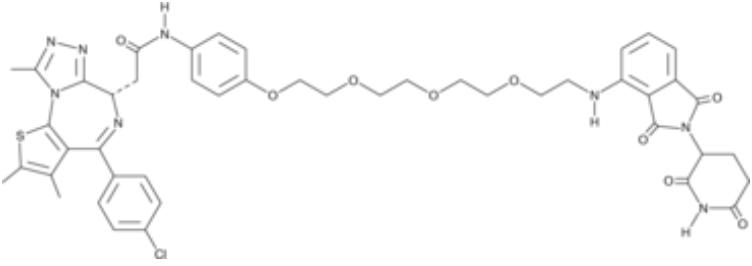
4 Development of Dual ARV-825 and Nintedanib - Loaded Nano-liposome for synergistic efficacy in Vemurafenib-resistant Melanoma

4.1 Drug

4.1.1 ARV-825

ARV-825 is a the first cereblon-based BRD4 PROTAC molecule that developed by researchers from Yale University and Arvinas [74]. It can specifically target BRD4 protein and showed faster and prolonged degradation of BRD4 protein compared to other BRD4 inhibitors. It is a hetero-bifunctional molecule composed of a ligand binding to the target protein BRD4 joined via an ethoxy spacer linker. Thienodiazepine part of ARV-825 recruits BRD4 directly to the E3 ubiquitin ligase cereblon, which binds to the phthalimide part of ARV-825. It has been previously revealed that ARV-825 exhibited promising efficacy for the treatment of vemurafenib-resistant melanoma, however, it was found as a substrate of CYP3A4 with short half-life [75]. According to Lipinski rule of five, the violations for ARV are two, which are number of hydrogen bond acceptor (should be less than 10 while ARV has 17) and molecular weight (should be less than 500 g/mole while ARV is 941 g/mole) [97]. Moreover, the polar surface area of ARV is 233 °A², whereas the polar surface area should be < 140 °A² for good oral absorption. Therefore, oral administration route may not be suitable for the delivery of ARV-825. Additionally, ARV is an extremely poor water-soluble molecule, which pose a significant challenge in development of translational parenteral formulation. The profile of ARV-825 was outlined in Table 7.

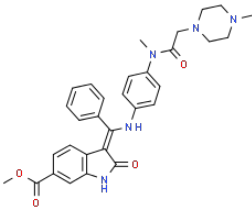
Table 7. ARV-825 drug profile

Name	ARV-825
Chemical Name	2-[(6S)-4-(4-Chlorophenyl)-2,3,9-trimethyl-6H-thieno[3,2-f][1,2,4]triazolo[4,3-a][1,4]diazepin-6-yl]-N-[4-(2-[98-dihydro-1H-isoindol-4-yl]amino)ethoxy) ethoxy] ethoxy} ethoxy) phenyl]acetamide
Molecular formula	C ₄₆ H ₄₇ ClN ₈ O ₉ S
Molecular weight	941.40 g/mol
Structure	
CAS No.	1818885-28-7
Description	ARV-825 is a hetero-bifunctional molecule which selectively degrades BRD4 protein. It is a yellow crystalline powder.
Partition coefficient	2.72
Solubility	N/A

4.1.2 Nintedanib

Nintedanib is a Food and Drug Administration (FDA) approved anti-fibrotic agent for the treatment of idiopathic pulmonary fibrosis in 2014 and along with other drugs like docetaxel for the treatment of non-small cell lung cancer. It was sold under the brand names Ofev and Vargatef that developed by Boehringer Ingelheim. Nintedanib was reported to inhibit vascular endothelial growth factor receptor (VEGFR) 1–3, platelet-derived growth factor receptor (PDGFR)- α and - β , and fibroblast growth factor receptor (FGFR) 1–3 [99]. Furthermore, nintedanib could inhibit ECM proteins like fibronectin, type I collagen and transforming growth factor (TGF)- β 1-induced myofibroblast transdifferentiation, all of which contribute to the reduction of dense network in the tumor extracellular matrix [100,101]. Nintedanib is reported as a substrate of the transporter P-glycoprotein, which transports the absorbed substance back into the gut's lumen [102]. Nintedanib was selected here as an anti-fibrotic agent and the uptake of nanotherapeutics would be increased due to the tumor stroma devastation by inhibiting (TGF)- β 1-induced fibroblast. The profile of Nintedanib was outlined in Table 8.

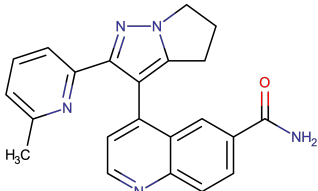
Table 8. Nintedanib drug profile

Name	Nintedanib
Chemical Name	4-(p-chlorophenyl)-4-hydroxy-N, N-dimethyl- a, a-diphenyl-1-piperidinebutyramide monohydrochloride
Molecular formula	C ₃₁ H ₃₃ N ₅ O ₄
Molecular weight	539.6 g/mol
Structure	 The chemical structure of Nintedanib is shown. It features a central benzimidazole ring system. One of the benzimidazole nitrogens is substituted with a 4-(p-chlorophenyl)-4-hydroxybutyl chain, which is further substituted with a dimethylpiperidine group. The other benzimidazole nitrogen is substituted with a phenyl group. The benzimidazole ring also has a methoxy group and a carbonyl group attached to the benzene ring.
CAS No.	656247-17-5
Description	Nintedanib is a small molecule tyrosine-kinase inhibitor. It is a bright yellow crystalline powder.
Melting point	244-251°C
Partition coefficient	3.0
Solubility	DMSO 25 mg/mL; Water <1 mg/mL
Half life	10-15 hours
Dosage	Dose: 100 mg and 150 mg
Indication and use	Anti-fibrotic/Anti-inflammatory Agent

4.1.3 Galunisertib

Galunisertib (LY2157299) is an oral small molecule experimental cancer drug in development by Eli Lilly. It is an inhibitor of the TGF β receptor I (TGF β RI) kinase that specifically downregulates the phosphorylation of SMAD2, abolishing activation of the canonical pathway [103]. Galunisertib is currently under clinical development of various type of diseases such as glioma, hepatocellular carcinoma, pancreatic cancer and Myelodysplastic Syndromes [104]. Galunisertib showed a prominent antifibrotic potency in a human ex vivo model of liver fibrosis [105]. The profile of Galunisertib was outlined in Table 9.

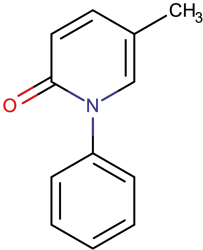
Table 9. Galunisertib drug profile

Name	Galunisertib
Chemical Name	4-[2-(6-methylpyridin-2-yl)-4H,5H,6H-pyrrolo[1,2-b] pyrazol-3-yl] quinoline-6-carboxamide
Molecular formula	C ₂₂ H ₁₉ N ₅ O
Molecular weight	369.42 g/mol
Structure	 <p>The chemical structure of Galunisertib is shown. It features a quinoline ring system with a carboxamide group (-CONH₂) at the 6-position. At the 4-position of the quinoline, there is a pyrrolo[1,2-b]pyrazole ring system. This pyrrolo[1,2-b]pyrazole is further substituted at its 2-position with a 6-methylpyridin-2-yl group, which consists of a pyridine ring with a methyl group (-CH₃) at the 6-position.</p>
CAS No.	700874-72-2
Description	Galunisertib is an anti-fibrotic agent. It is a grey to brown solid powder.
Solubility	Water 0.0112 mg/mL
LogP	3.11
Polar Surface Area	86.69 Å ²
Half-life	8.6 h

4.1.4 Pirfenidone

Pirfenidone is an orally administered drug with antifibrotic, anti-inflammatory, and antioxidant effects [106]. It approved by FDA on 2014 as a medication for the treatment of idiopathic pulmonary fibrosis under the brand name Esbriet [107]. *In vitro* evidence has shown that pirfenidone inhibits collagen synthesis, fibronectin synthesis, fibroblast, epidermal, platelet-derived, and transforming beta-1 growth factors, thereby slowing tumor cell proliferation [108-110]. Pirfenidone has demonstrated activity in various fibrotic conditions such as lung, kidney and liver [111]. The profile of Pirfenidone was outlined in Table 10.

Table 10. Pirfenidone drug profile

Name	Pirfenidone
Chemical Name	5-methyl-1-phenyl-1,2-dihydropyridin-2-one
Molecular formula	C ₁₂ H ₁₁ NO
Molecular weight	185.22 g/mol
Structure	
CAS No.	0053179-13-8
Description	Pirfenidone is potent TGFβ receptor I (TβRI) inhibitor. It is a white solid powder.
Solubility	Water 2.89 mg/mL
Dosage forms	Capsule, Tablet
Administration route	Oral
Half-life	2-2.5h
LogP	2

4.2 Materials

ARV was obtained from ChemieTek (Indianapolis, IN, USA), Ni and Vemurafenib was purchased from LC Laboratories (Woburn, MA, USA), 1,2-Dioleoyl-sn-glycero-3 phosphocholine (DOPC) was purchased from Cordenpharma (Liestal, Switzerland), PE 18:0/18:0-PEG2000 was obtained from Lipoid (Ludwigshafen, Germany), Cholesterol and Chloroform were purchased from Sigma-Aldrich (MO, USA), The TGFβ1 ELISA kits were purchased from Invitrogen (Carlsbad, California, USA). Dulbecco's modified Eagle's medium (DMEM) was purchased from ThermoFisher Scientific Inc. (Waltham, MA, USA), Fetal Bovine Serum (FBS) was procured from Atlantic Biologics (Oakwood, GA, USA). Penicillin-Streptomycin-Amphotericin B (PSA) was purchased from MP Biomedicals, LLC (Solon, Ohio, USA). MTT (3-(4,5-dimethylthiazol-2-yl)-2,5-diphenyl tetrazolium bromide) was acquired from Fisher Scientific. Other chemicals and solvents were of analytical grade or chromatographic purity.

Melanoma cell lines (A375 and Sk-Mel-28) were purchased from American Type Culture Collection (Manassas, Virginia, USA). Vemurafenib-resistant melanoma cell lines (A375R and SK-MEL-28R) was developed by adding vemurafenib to the cell line as the method described before (REF). The vemurafenib resistance was confirmed prior to studies. GFP expressing human dermal fibroblasts (HDFCs-adGFP) were obtained from angio-proteomie (Boston, MA, USA). Cells were cultured in DMEM medium supplemented with 10% fetal bovine serum (FBS) at 37°C with 5% CO₂ in humidified incubator.

4.3 Methods

4.3.1 Analytical Method (HPLC method development)

Chromatographic separation method of ARV and Ni was developed using Waters e2695 separation module, equipped with 2998 Photo diode array (PDA) detector and Hypersil ODS C18 column (250mm × 4.6 mm, 5 μ m). The mobile phase was Acetonitrile:Potassium dihydrogen phosphate buffer (10 mM) of pH 3.5 (70:30) with a flow rate of 1 mL/min. The temperature of the column was kept at 25 °C and Empower 3 software was used to monitor output signal. ARV was detected at 247 nm and Ni was detected at 390 nm. The retention time of ARV and Ni were 4.48 \pm 0.02 min and 9.15 \pm 0.36 min, respectively.

4.3.2 Enzyme Linked Immunosorbent Assay

The enzyme linked immunosorbent assay (ELISA) kit was used to determine the level of TGF- β 1 secreted by A375, SK-MEL-28, A375R and SK-MEL-28R and 3D spheroids. For 2D culture, cells were seeded at 1.2×10^4 cells per well in a 24-well plate and incubated at 37°C with 5% CO₂. Cells were harvested when 90% confluency was reached. Then the supernatants were collected by centrifugation at 1,000 x g for 10 min at 4°C. For 3D spheroid culture, the supernatant in each well was taken on the 6th day before treatment. Three independent experiments were conducted in duplicate according to the manufacture's protocol. Briefly, 100 μ L of sample or TGF- β 1 standard protein per well was incubated for 2 h at room temperature in ELISA plate that coated with capture antibody. Afterward, the samples were completely washed and 100 μ L TGF- β 1 detection antibody was added to each well for 1 h incubation followed by incubation with Avidin-HRP and tetramethylbenzidine (TMB) substrate. Finally, after adding stop solution, the optical density (OD) values of different samples were detected at 450nm by using a microplate reader (Dynex Technologies). The concentration of TGF- β 1 was interpolated using a second-order polynomial (quadratic) equation generated from a standard curve in GraphPad Prism 7.

4.3.3 Cell viability assay and effect of drug combination

The cytotoxicity of ARV, Ni and ARNIPL were evaluated in A375R and SK-MEL-28R using 3-(4,5-dimethylthiazol-2-yl)-2,5-diphenyl tetrazolium bromide (MTT) assay. Logarithmic growth phase cells were seeded in 96-well plates at a density of 5000 cells/well. After 24 h, drugs and formulation were diluted in cell culture medium to achieve different concentrations. After 48 h treatment, cells were incubated with 20 μ L of 5 mg/mL MTT solution in each well and incubated for 3 h at 37 $^{\circ}$ C, 5% CO₂. Then the medium was removed and MTT-formazan crystals were dissolved by adding 100 μ L of dimethyl sulfoxide (DMSO) to each well. The quantity of MTT-formazan was determined by 570 nm absorbance on an Epoch2 microplate. IC₅₀ were calculated using GraphPad Prism7 Software.

Effect of ARV and Ni combination was assessed and according to Combination index (Chou-Talalay method) and Combenefit software (48). Following equation was used to calculating combination index (CI):

$$CI = (D)1/(Dx)1+(D)2/(Dx)2$$

where (Dx) 1, (Dx) 2 = the concentration of the tested substance 1 and the tested substance 2 used in the single treatment that was required to decrease the cell number by 50% and (D) 1, (D) 2 = the concentration of the tested substance 1 in combination with the concentration of the tested substance 2 that together decreased the cell number by 50%.

4.3.4 Preparation of ARNIPL

Modified hydration method was used for the preparation of ARNIPL. Briefly, ARV: Ni: DOPC: cholesterol: DSPE-PEG2000: citric acid in a 1:3.5:45:15:2 molar ratio was dissolved in chloroform. Parenteral-grade mannitol (200 μ m) was used as absorbent and the chloroform solution was drop-wise added to mannitol with constant stirring at 45°C. The resultant paste was left overnight for chloroform evaporation. The resultant powder was dispersed in water contains citric acid at 55°C followed by sonication (30% amplitude) for 2 min. The same method was employed for the preparation of liposome without citric acid for comparison.

4.3.5 Characterization of ARNIPL

The average size, size distribution by intensity, zeta potential of ARNIPL were measured using dynamic light scattering (DLS) particle size analyzer (Malvern Zetasizer Nano ZS, Royston, UK). Samples were analyzed using disposable cuvettes at 25°C with a scattering angle of 173°. Amicon ultra centrifugal filters (50K) were used to analyze the entrapment efficiency of ARNIPL. The sample of total and free drug were collected and the concentration was analyzed by HPLC. The encapsulation efficiency was calculated using the following formula:

$$\text{Percent encapsulated} = ([\text{Total drug}] - [\text{Free drug}]) / [\text{Total drug}] \times 100\%$$

4.3.6 Stability study

ARNIPL prepared by modified hydration method were used for the stability study. Particle size, zeta potential, drug content and entrapment efficiency after one month of storage at 4 °C were evaluated. Samples were withdrawn at different time points after centrifugation of ARNIPL at 5000 rpm for 10min. The concentration of drug at each time points were analyzed using HPLC. The percentage drug content was plotted at different time intervals.

4.3.7 *In Vitro* Release Study

Drug release from ARNIPL was carried out using the dialysis bag method. Dialysis bags (Spectra/Por® 7) were soaked in Milli-Q water at room temperature overnight to remove the preservative. Release of ARV and Ni were carried out at 37 °C in a dialysis sac with 100 mL of phosphate buffer saline (pH 7.4) containing 0.5% TPGS with constant stirring. The samples were withdrawn from the release medium at different time intervals up to 48 h. The concentration of ARV and Ni in the release media was evaluated by HPLC. The percentage of release of each drug was plotted versus time points.

4.3.8 Clonogenic assay

Clonogenic assay was carried out according to the procedure described previously (49). A375R were seeded at a density of 1000 cells/well in a 6-well plate. The cells were allowed to attach for around 5 h. Then the cells were treated with ARV (0.2 μM), Ni (0.7 μM) and ARNIPL (ARV 0.2 μM and Ni 0.7 μM) before the population doubling. The next day, the medium was replaced and cells were maintained at 37°C with 5% CO₂ for 5 days. Then cells were rinsed with PBS followed by glutaraldehyde (6.0% v/v) fixation and 0.5% crystal violet staining for 30 min. Thereafter, the plate was washed with water and left for drying. Colonies were counted (the colony is defined to consist of at least 50 cells) on the following day. Plating efficiency (PE) and survival fraction (SF) was calculated by following equations:

$$\text{PE} = \text{number of colony formed} / \text{number of cells seeded} \times 100\%$$

$$\text{SF} = \text{PE of treated sample} / \text{PE of control} \times 100$$

4.3.9 Vasculogenic mimicry

A375R cells suspension at 2×10^5 /ml were incubated with ARV (0.2 μ M), Ni (0.7 μ M) and ARNIPL (ARV 0.2 μ M and Ni 0.7 μ M) for 5 min at 37°C followed by seeding in a 96 well plate precoated with 50 μ L BME at a density of 2×10^4 /well. After 24 h incubation at 37 °C with 5% CO₂, images were taken using an EVOS light microscope at 20 \times . Number of branching points were quantified for tube formation.

4.3.10 Flow cytometry for apoptosis analysis

A375R were seeded at a density of 1×10^5 /mL in 6-well plate and cells were treated with ARV (1 μ M), Ni (3.5 μ M), ARNIPL (contains ARV 1 μ M and 3.5 μ M Ni) for 24 h incubation. Then cells were collected by centrifugation at 3000 rpm for 5 mins and resuspended with DMEM media (contains 1% bovine serum albumin and 1% FBS) to a concentration of 5×10^5 cells/mL. Apoptosis analysis was carried out by Muse Annexin V & Dead Cell Assay kit (Millipore Sigma, USA). Briefly, the cell suspension was diluted in 1:1 ratio with MUSE Annexin V dead cell reagent, followed by incubated for 20 mins at room temperature, then the samples were analyzed for apoptosis using Muse® Cell Analyzer (MilliporeSigma, USA).

4.3.11 Determination of ARNIPL Efficacy in 3D Spheroids

4.3.11.1 Development and characterization of 3D multicellular tumor spheroids

Tumor spheroid of A375R alone and co-culture of A375R + dermal fibroblast (1:0.5) were prepared as follow; Briefly, cells were seeded at a density of 1500 cells/well in ultra-low attachment treated spheroid microplate (Corning Life Sciences, MA, USA). The plate was centrifuged at 150×g for 10 min and incubated overnight. The cells were then treated with ARV, Ni, ARNIPL and ARV+Ni with 1 μM ARV and 3.5 μM Ni in each group. Media was added as a control. The media was replaced with fresh treatment every alternative day until day 6. Moreover, same treatment groups with higher concentration (2 μM ARV and 7 μM Ni) were also investigated in co-culture spheroids and treated until day 4. Images of 3D spheroids were taken at 20× magnification every time before treatment using EVOS® FL Auto Imaging System (Thermo Fisher Scientific, Waltham, MA, USA).

4.3.11.2 3D cell viability study

The viability of 3D spheroids was analyzed using CellTiter-Glo kit (Promega, Madison, WI, USA). After imaging on day 7 of treatments, equal volume of CellTiter-Glo® reagent was added in the well (100 µL of CellTiter-Glo® reagent and 100 µL of cell culture media in each well) and the plate was vigorously shaken for 5 minutes to induce cell lysis, followed by incubation at room temperature for 25 minutes to stabilize the luminescent signal. The luminescence was then measured using a Spark 10M plate reader (Tecan, Männedorf, Switzerland).

4.3.11.3 3D spheroid live & dead cell imaging

On the 7th day of treatment, spheroids were washed twice with phosphate-buffered saline (PBS) followed by staining with 3 μ M EthD-1 and 1 μ g/mL DAPI (Santa Cruz Biotechnology, TX, USA) in PBS solution. The plate was incubated at 37°C for 3 h and fluorescent images were then taken at 20 \times using EVOS-FL Cell Imaging fluorescence microscope (Thermo Fisher Scientific, Waltham, MA, USA).

4.4 Results and Discussion

4.4.1 Analytical Method (HPLC)

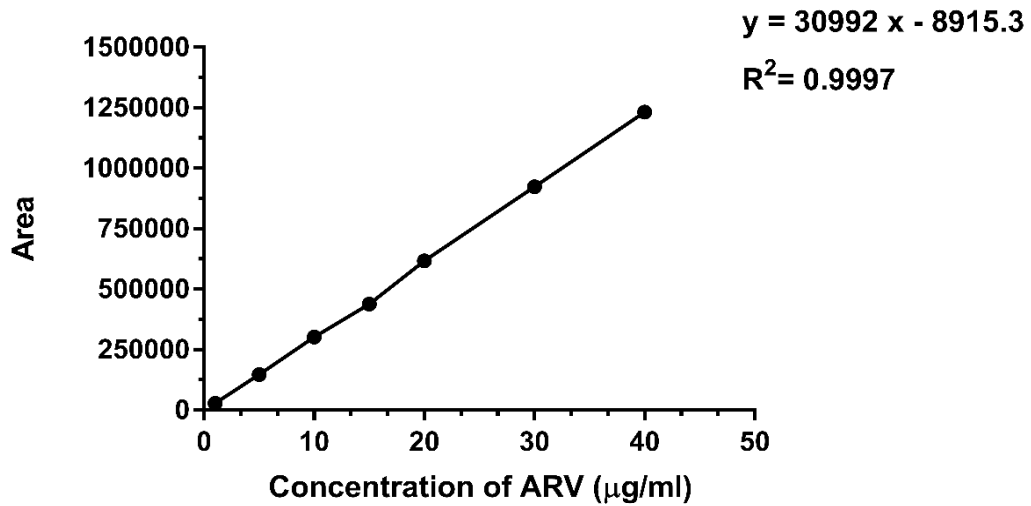


Figure 13. Standard curve of ARV.

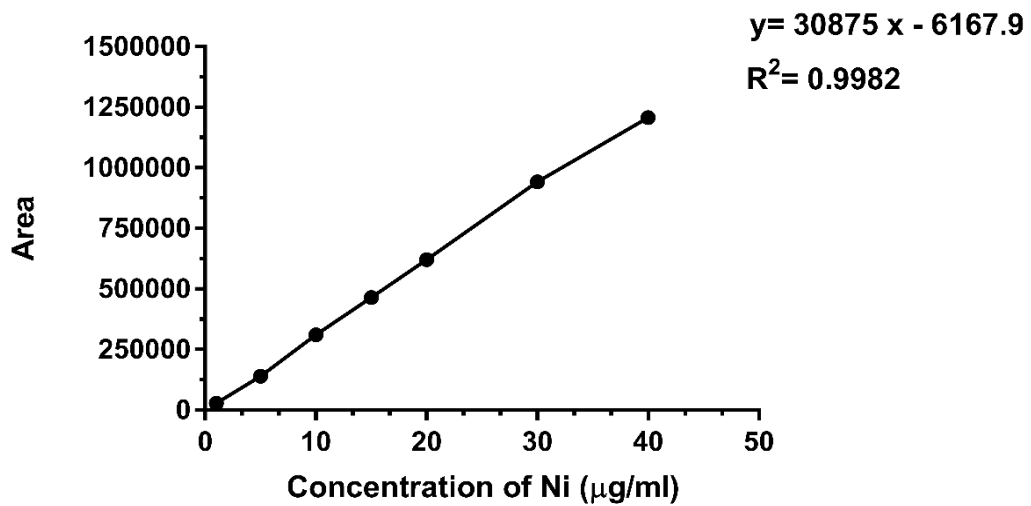


Figure 14. Standard curve of Ni.

4.4.2 Enzyme Linked Immunosorbent Assay

In order to investigate whether TGF- β 1 production is more in the vemurafenib-resistant melanoma cells than BRAF^{V600E} mutated melanoma cell lines, two BRAF^{V600E} mutated melanoma cell lines A375 and SK-MEL-28 and their vemurafenib-resistant cells lines were used in ELISA assay to compare the amount of TGF- β 1 release from the same number of cells. The result shown in Figure 15 revealed that a significant increasing amount TGF- β 1 was found in the vemurafenib-resistant cell lines, which suggested the potential of targeting TGF- β 1 in vemurafenib-resistant melanoma.

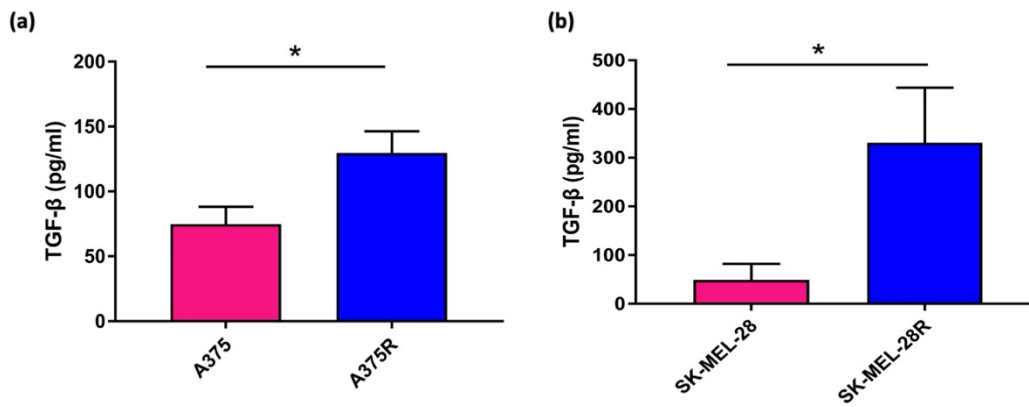


Figure 15. ELISA analysis of TGFβ1 produced by BRAF^{V600E} mutated melanoma cell lines and its vemurafenib-resistant cell lines. Results are expressed as the amount (pg)/mL of TGFβ1 produced by the same number of cells of (a) A375 and A375R, (b) SK-MEL-28 and SK-MEL-28R. Data shown are the means ± SD (n = 3). (*p< 0.05)

4.4.3 Cell viability assay and effect of drug combination

The effect of drug combination was analyzed using Combenefit software. The contour plot of synergy/antagonism with the Bliss model was shown in Figure 16. The positive scores mean the drug combination are synergistic while the negative scores indicated the combination was antagonist. All positive scores were observed in A375R while in SK-MEL-28R, the scores are less with lighter blue color. The result suggested that the synergistic effect was stronger of ARV and Ni in A375R compared with SK-MEL-28R. Thus, the further anti-cancer efficacy studies of ARNIPL were evaluated in A375R. As shown in Figure 17, Free Ni and ARNIPL killed cells in dose-dependent manners. However, ARV did not show further killing above 1 μ M, which can be explained by “hook effect” and resulted in a bell-shaped dose-response curve of the PROTAC molecules. This phenomenon is attributed to the mechanism of the PROTAC molecule, which tends to form a binary complex with either E3 ligase or protein of interest instead of forming ternary complex at higher concentration [112]. Nevertheless, the combination of Ni with ARV may not only serve a dual-functional targeting purpose, but also alleviate the limitation of “hook effect”. On the other side, ARV dominate the killing at very low concentration while Ni did not show too much killing. However, with the increasing of concentration, Ni showed promising killing of melanoma cells and the combination with ARV in ARNIPL further decrease the viability. Additionally, the IC₅₀ of ARV and Ni in the liposomes were lower than the free drug (Table 11). The calculated combination index (CI) of ARV and Ni was 0.54 ± 0.05 while the CI of ARNIPL showed 0.59 ± 0.12 , indicating there is synergism between Ni and ARV and the synergism remains similar in ARNIPL.

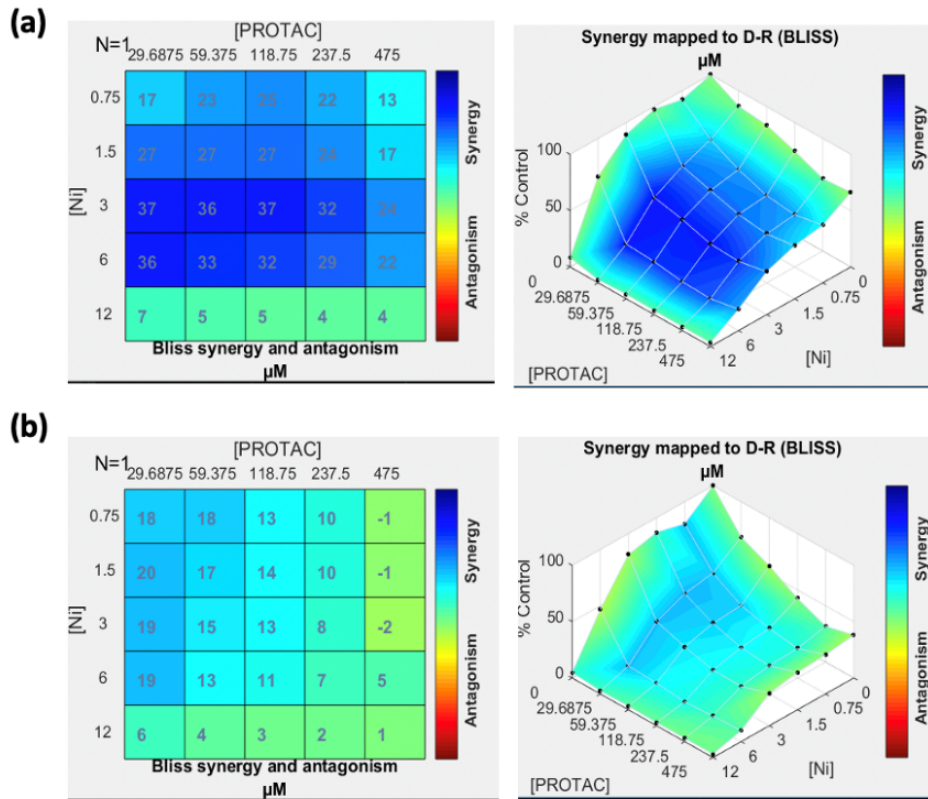


Figure 16. Combenefit mapped surface output for the drug combinations involving ARV and Ni using Bliss synergy model. ARV and Ni synergistically inhibit cell growth in a panel of (a) A375R and (b) SK-MEL-28R. Cells were treated with ARV and Ni in a 5x5 concentration grid for 48 h, cell viability was determined by MTT assay. The darker the blue color, the more predicted synergy between the drugs (n=3).

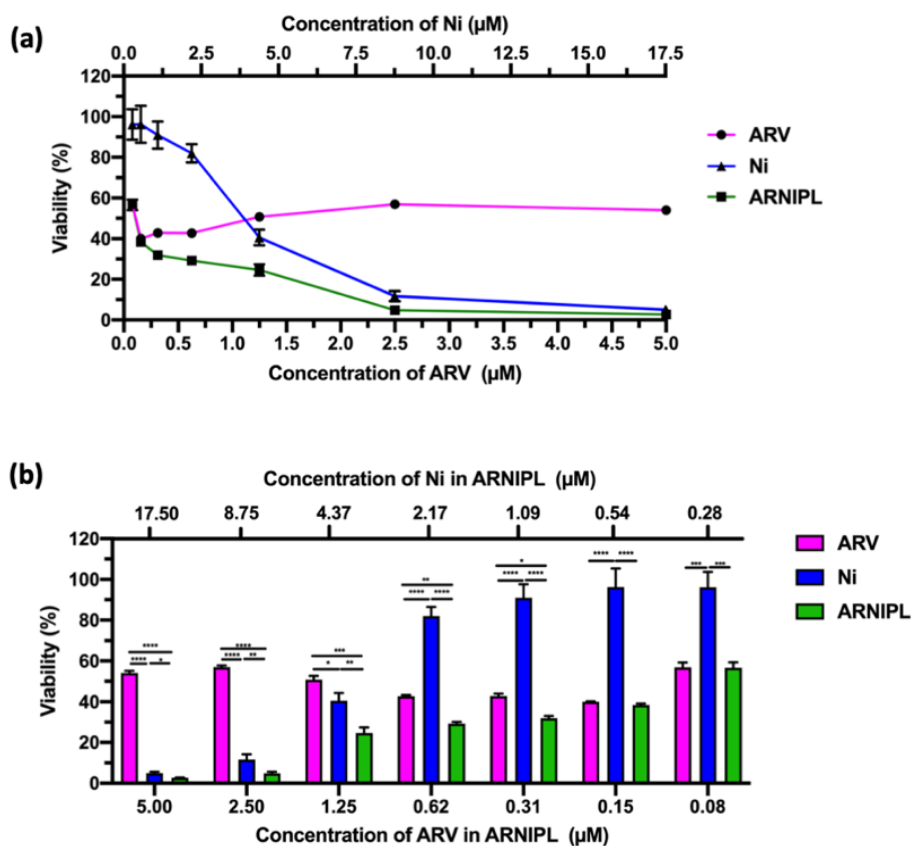


Figure 17. Cytotoxicity assay of ARV, Ni and ARNIPL in A375R. (a) % Cell viability with ARV, Ni and ARNIPL treatment in A375R. (b) The % viability comparison of ARV, Ni and ARNIPL at various concentrations. Data was plotted as mean \pm SEM (n=3).

Table 11. *In vitro* cytotoxicity of Ni, ARV alone and in the liposomes in A375R (n=3).

Drug	Ni	ARV	ARNIPL-Ni	ARNIPL-ARV
IC ₅₀ (µM)	4.35 \pm 0.47	0.13 \pm 0.08	0.07 \pm 0.06	0.24 \pm 0.05

4.4.4 Characterization

Due to the poor entrapment efficiency (EE) and drug loading (DL) of ARV and Ni, citric acid was incorporated in the hydration step to enhance the EE and DL via interaction of citric acid with basic drugs. Weak acids or weak bases are used in the formulation development for solubility and stability enhancement. Due to the basic property of the drugs, we selected citric acid due to its safe use in parenteral delivery. Initially, 1% ARV and 2% Ni were aiming to be loaded into the liposomes, the EE without citric acid of ARV and Ni were 79.68%, 21.67% respectively, while the result in more than 90% EE of both of the drugs with the citric acid. Moreover, the DL of ARV and Ni was also increased with citric acid (Table 12). Thereafter, we prepared batches with high DL and high concentration of ARV and Ni. The particle size and zeta potential of optimized ARNIPL are shown in Figure 18, the mean particle size of ARNIPL is 111.1 ± 6.97 nm, which is in the range of enhanced and permeation (EPR) effect that allows particles to easily extravasate into tumors. The polydispersity index was less than 0.3, which indicates the particles were uniformly distributed. The zeta potential of ARNIPL was found to be $+13.9 \pm 6.62$, which may mainly attribute to the orientation of basic (amine group) towards surface of ARNIPL with lipophilic part entangled in lipid bilayer. This arrangement is similar to the cholesterol in the membrane, where eight-carbon branched aliphatic tail located in the membrane whereas the polar hydroxyl group was left outside [113]. Moreover, the head group-modified lipids with amine is also exposed on the outside surface of the liposomes [114].

Table 12. Particle size, zeta potential and entrapment efficiency (EE) of ARNIPL (n=3).

Group	Size (nm)	Zeta potential (mV)	EE of ARV(%)	EE of Ni(%)	DL of ARV(%)	DL of Ni(%)
ARNIPL (without citric acid)	138.4 ± 6.66	-25.2 ± 4.41	79.68 ± 7.60	21.67 ± 2.15	0.80 ± 0.08	0.43 ± 0.04
ARNIPL (with citric acid)	99.62 ± 4.78	-5.34 ± 3.82	94.15 ± 3.48	97.16 ± 2.33	0.94 ± 0.03	1.94 ± 0.05
ARNIPL (optimized)	111.5 ± 6.55	+12.1 ± 5.61	97.80 ± 3.20	96.86 ± 2.63	1.96 ± 0.05	3.87 ± 0.11

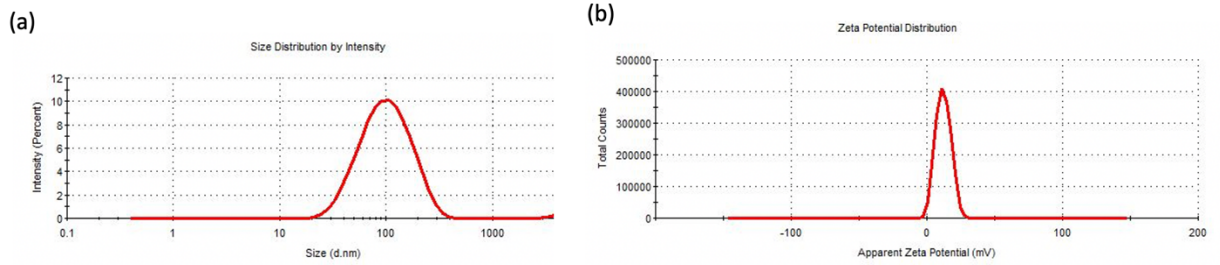
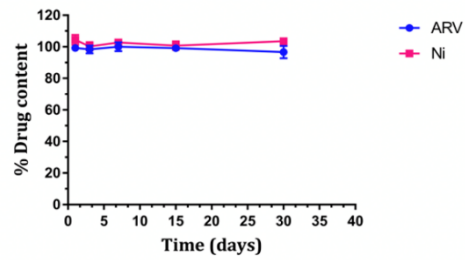


Figure 18. ARNIPL characterization. (a) Particle size distribution with an average diameter of 111.5 ± 6.55 nm (b) zeta potential of ARNIPL.

4.4.5 Stability study

Physical stability of ARNIPL prepared by modified hydration method was analyzed after a month storage at 4°C. ARNIPL was found to be physical stable for one month at 4°C storage (Figure 19 (a)), which indicated the ARNIPL was stable after a month storage. Moreover, the particle size of ARNIPL was 111.5 ± 6.55 with polymer dispersity index less than 0.25 and zeta potential was found to be 12.1 ± 5.61 mV (Figure 19 (b)).

(a)



(b)

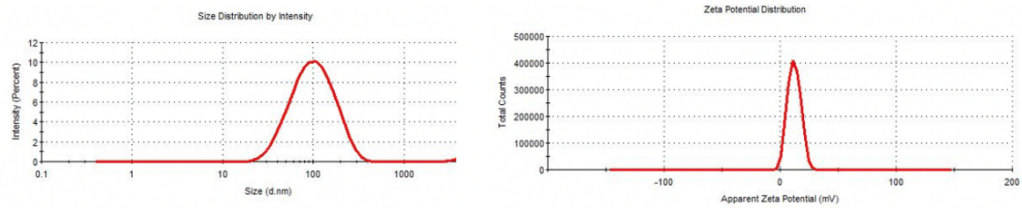


Figure 19. The stability result of ARNIPL. (a) Drug content after a month storage at 4°C. The data of each time point was conducted in triplicate and was shown as mean with standard deviation. (b) Particle size and zeta potential of ARNIPL after a month storage at 4°C.

4.4.6 *In Vitro* Release Study

The release of ARNIPL was detected by HPLC at 1 h, 2 h, 4 h, 6 h, 8h, 24h and 48 h. Sink condition was maintained during the study using a non-ionic surfactant 0.5% TPGS in the release medium. The result showed less 2% of ARV and less than 5% of Ni was released in 24 h. After 48 h, the percentage release of both drugs was increased but still within 5% for ARV and less than 10% for Ni at sink conditions (Figure 20), which indicated that the ARNIPL did not show any burst release of ARV and Ni.

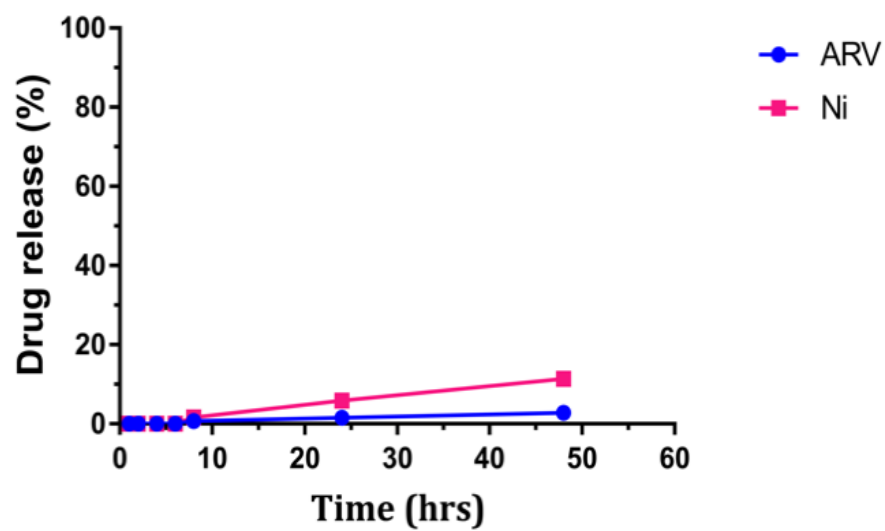


Figure 20. *In vitro* release study of ARNIPL. Release of ARV and Ni were observed at pH 7.4 in sink condition. Data are expressed as mean and standard deviation.

4.4.7 Clonogenic assay

The ability to form colonies after treatment was analyzed by clonogenic assay, which also determines cell reproductive death after treatment. Results as shown in Figure 21 suggested that the number of colonies were significantly reduced by the exposure to Ni and ARV alone group. ARNIPIL showed 8-20 folds lesser number of colonies compared to drug alone and control group. Plating efficiency (PE) of A375R control was 40 %. Survival fraction (SF) of ARNIPL was much lower compared to other treatment groups as shown in Table 13. ARNIPL exhibited more predominant inhibition of melanoma cells to form colonies, which is in accordance with our cytotoxicity suggesting that the combination of drugs exerted synergistic effect in melanoma tumor inhibition. Moreover, TGF- β 1 was found to related with regulating clonogenicity of melanoma cells and TGF- β 1 inhibition could block the clonogenicity through SMAD4-independent inhibition of mitosis [115]. Thus, the effect of Ni in clonogenicity assay could related with TGF- β 1 pathway.

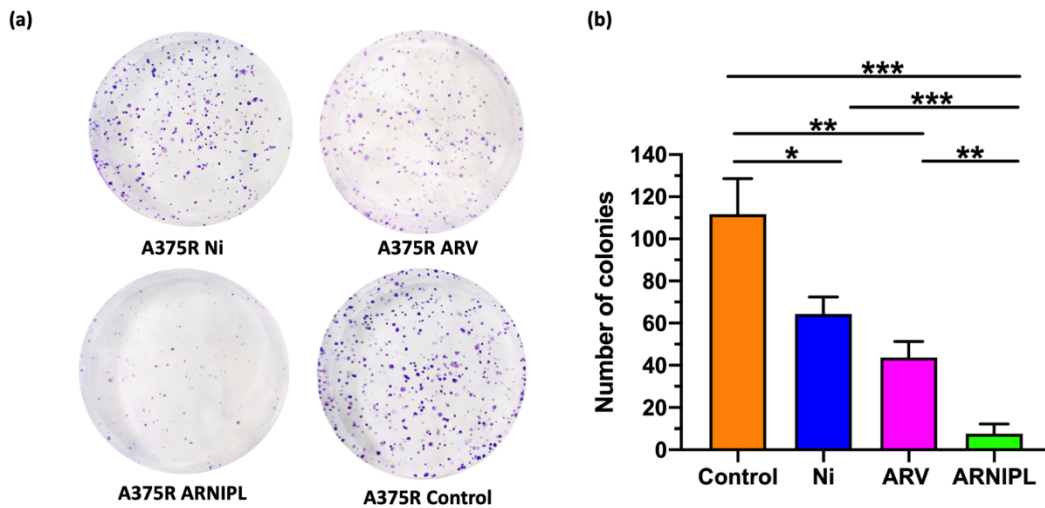


Figure 21. Colony forming ability of A375R after treatment with ARV, Ni and ARNIPL
 (a) Crystal violet staining images of A375R after various treatments. (b) Number of colonies with ARV, Ni and ARNIPL treatment and control in A375R. Number of colonies with ARNIPL treatment were significantly reduced compared to other groups (* $p < 0.05$, ** $p < 0.01$, *** $p < 0.001$).

Table 13. Clonogenic Assay: Surviving Fraction (SF) of treatment cells

(n = 3); S.D. = Standard deviation.

%SF ± S.D.	Ni	ARV	ARNIPL
A375R	47.5 ± 4.19	37.5 ± 3.81	18.0 ± 2.25

4.4.8 Vasculogenic mimicry

Melanoma vasculogenic mimicry was first described and characterized by Maniotis group, where the tube formation was distinct from endothelial cells [116]. Vasculogenic mimicry is a different vascular formation mechanism compared to traditional angiogenesis, which is formed by tumor cells and independent of endothelial cells. The tube formation by vasculogenic mimicry that observed in aggressive tumors provides sufficient blood perfusion and nutrition to the tumor, which is related to the poor survival [117]. The formation of vasculogenic mimicry was observed in A375R on the Matrigel. ARV and Ni inhibited vasculogenic mimicry at very low concentration as shown in Figure 22 (a). ARNIPL containing ARV and Ni showed further inhibition of vasculogenic mimicry compared to each individual drug. The number of branching points are plotted in Figure 22 (b), where ARV and ARNIPL both showed most significantly lower number of branching points. There was no statistically significant difference between ARV and ARNIPL. We previously demonstrated that ARV has promising effect in the inhibition of vasculogenic mimicry in A375R [118]. In the present paper, Ni was also able to inhibit vasculogenic mimicry. This may be due to inhibition of multiple signaling pathway, which was reported to be a potential target for anti-vasculogenic mimicry in cancer [119]. ARNIPL displayed the most predominant anti-vasculogenic mimicry effect in A375R.

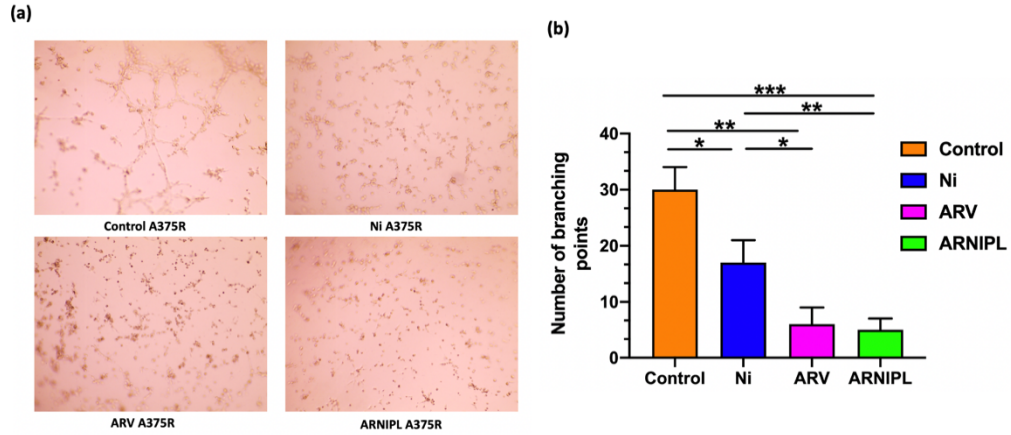


Figure 22. Evaluating the effect of ARNIPL on A375R vasculogenic mimicry (a) Vasculogenic mimicry images of A375R treated with ARV (0.2 μM), Ni (0.7 μM) and ARNIPL (ARV 0.2 μM and Ni 0.7 μM). (b) Number of branching points after treated with ARV, Ni and ARNIPL treatment in A375R. Data were expressed as mean \pm S.D. ARNIPL shows significantly less number of branching points compared to other treatment group. (* $p < 0.05$, ** $p < 0.01$, *** $p < 0.001$).

4.4.9 Apoptosis assay

Apoptosis of vemurafenib-resistant melanoma cell line A375R was carried out by flow cytometry, which shows percentage of early and late apoptosis distribution of the treated cells. The total apoptosis was calculated as the sum of early apoptosis and late apoptosis. Total apoptosis of Ni, ARV, ARNIPL and ARV+Ni is shown in Figure 23, where ARNIPL and the combination of ARV and Ni showed significantly higher amount of apoptosis compared to ARV and Ni alone. As expected, there was no difference in number of apoptotic cells in ARV+Ni (Added from DMSO stock) and ARNIPL (Same concentration added as liposomal formulation). As for the result of apoptosis assay, ARNIPL and ARV+Ni groups showed higher population of early/late apoptosis compared to single ARV or Ni treatment. The apoptotic effect of ARV was reported as a result of disrupting BRD4 that is expressed in various type of cancer [120-122]

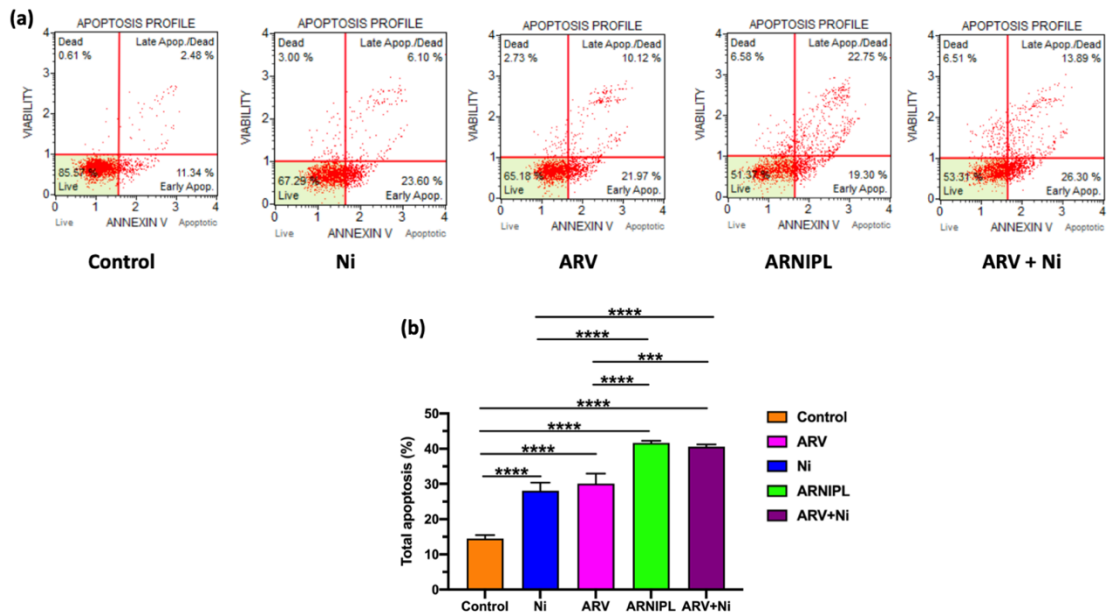


Figure 23. Flow cytometric analysis in A375R treated with 3.5 μM Ni, 1 μM ARV, ARNIPL and ARV+Ni (3.5 μM Ni and 1 μM ARV) after 24 h treatment, ARNIPL showed higher apoptotic cell population compared with control. (** $p < 0.001$, **** $p < 0.0001$).

4.4.10 Determination of ARNIPL Efficacy in 3D Spheroids

4.4.10.1 Development and characterization of 3D multicellular tumor spheroids

In order to better mimic *in vivo* tumor growth, 3D multicellular tumor spheroids of A375R and co-culture spheroids with dermal fibroblasts were developed to evaluate the efficacy of ARNIPL. According to the bright field images of A375R and co-culture spheroids with different treatments on days 0, 2, 4, and 6 as shown in Figure 24 (a) and (b), the growth of co-culture spheroids was found to be much faster than the spheroids that only contains A375R. The spheroid growth-promoting effect from fibroblasts co-culture has previously been discussed due to the role of fibroblasts in tumor progression [123]. The reduction of tumor spheroids with Ni and ARV at low concentration suggested the drugs are very potent. Moreover, the killing pattern of ARV and Ni observed from the surface of the spheroids was different. The killing effect of ARV can be observed on the surface, as seen from the irregular surface of the spheroids on day 6, which means ARV inhibits tumor growth by killing melanoma cells from the surface. As for the Ni treatment, the spheroids surface remains regular round shape and showed more intact smooth surface while the tumor growth has been inhibited, which implied the growth inhibition could be related with the regulation of melanoma cells through various signaling pathways. For instance, Ni could inhibit multiple factors and reduce CAFs through TGF- β 1 inhibition, which affects the proliferation of melanoma cells. Ni treated groups also showed dark and dense core, which may be due to the apoptotic cells present on the periphery of the spheroids [124]. The surface of combination of spheroids treated with both drugs in ARNIPL and ARV+Ni was uneven and showed better inhibition in tumor volume compared to individual drugs, this further confirmed the importance of drug

combination and could be related with synergistic effect of ARV and Ni. As for A375R spheroids growth as a function of time (Figure 24 (c)), Control and Ni group exhibited constant growth till day 6 and Ni showed slower growth compared to control. ARV, ARNIPL and ARV+Ni treated groups showed substantial inhibition of tumor growth compared with control. The volume of A375R spheroids with various treatments were compared on day 6 as shown in Figure 24 (e), all the treatment groups showed significant tumor volume reduction compared with control. Precisely, ARV treated group displayed more reduction of tumor volume than Ni treated group, and the combination of both drugs in ARNIPL and ARV+Ni further decreased the volume of the spheroids. Moreover, ARNIPL treated groups presented lower tumor volume compared with ARV+Ni, which may be due to the better penetration of the liposomes. The reduction of volume with ARV, Ni, ARNIPL and ARV+Ni treatment compared to control were 41.34%, 9.60%, 51.71% and 36.19%, respectively. The volume of the co-culture spheroids with various treatments as a function of time were shown in Figure 24 (d), spheroids showed rapid growth in control and Ni treated groups while other treatment groups showed significant inhibition in terms of tumor growth. The tumor volume of various treatments was compared at day 6 as shown in Figure 24 (f) where all the groups showed significant tumor inhibition compared with control. On day 6, The reduction of volume with ARV, Ni, ARNIPL and ARV+Ni treatment compared to control are 57.14%, 7.14%, 71.43% and 71.43%, respectively. ARV treated group exhibited more inhibition than Ni treated group in terms of tumor volume. And the combination group of drugs in ARNIPL and ARV+Ni showed further reduction of tumor volume compared to individual drugs. No

significant difference in tumor volume was observed in ARNIPL compared to ARV+Ni in 3D co-culture spheroids on day 6.

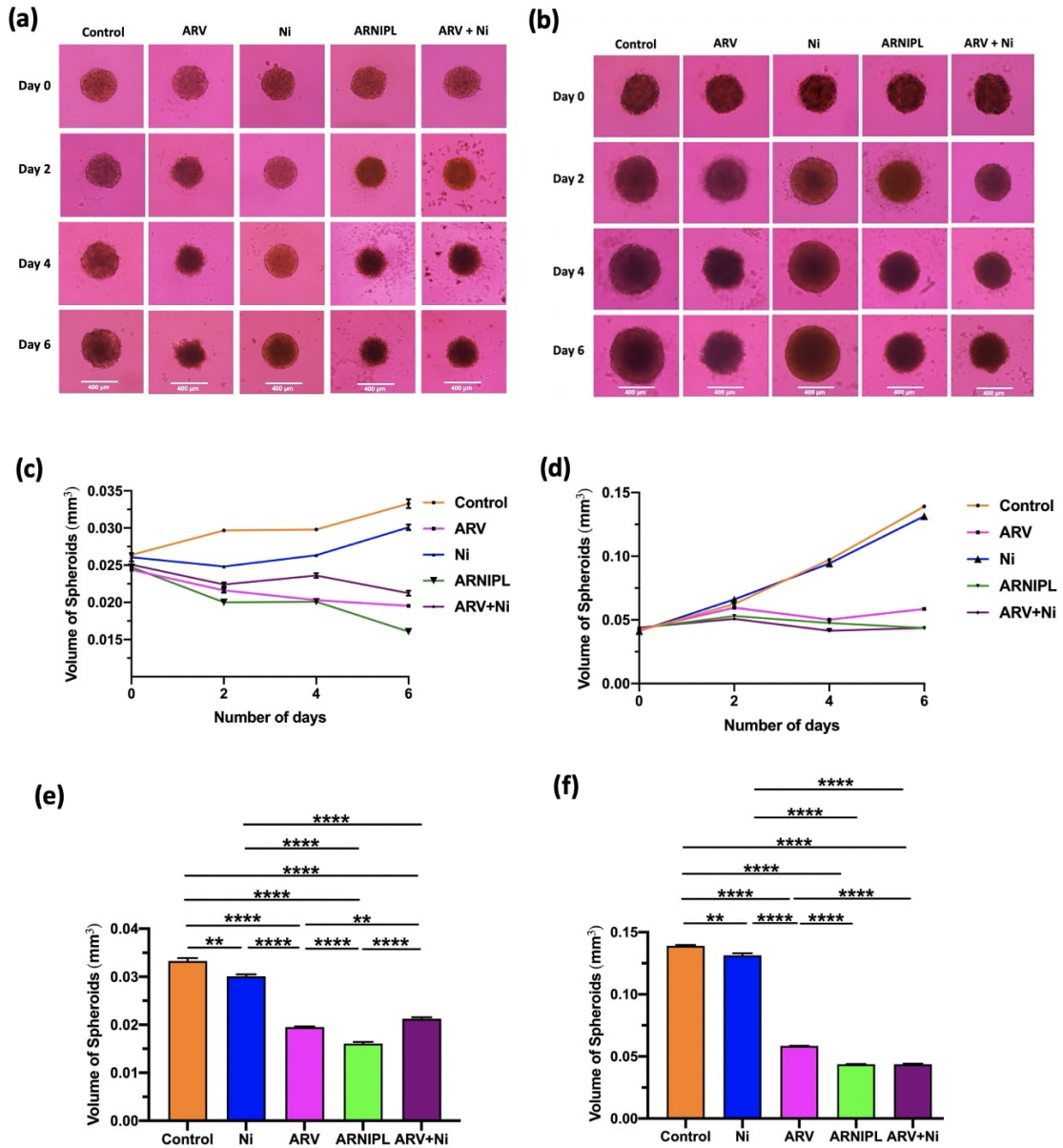


Figure 24. The effect of various treatments on A375R and A375R+Dermal Fibroblast co-culture 3D multicellular tumor spheroids growth. Spheroids were treated with control, 1 μM ARV, 3.5 μM Ni, ARNIPL and ARV+Ni (1 μM ARV and 3.5 μM Ni) (a) Bright field images of A375R spheroids with treatments on days 0, 2, 4, and 6. (b) Bright field images of co-culture spheroids with treatments on days 0, 2, 4, and 6. (c) Comparison of

the volume of A375R spheroids. (e) Comparison of the volume of co-culture spheroids with various treatments at day 0, 4 and 6. (f) The volume of A375R spheroids on day 6. (f) The volume of co-culture spheroids on day 6. Significant difference in volume of spheroids was observed with ARV, Ni, ARNIPL and ARV+Ni compared to control. (**p < 0.01, ***p < 0.001, ****p < 0.0001).

4.4.10.2 3D cell viability study

The CellTiter-Glo luminescent cell viability assay was performed to study the number of viable cells in treated A375R and co-culture spheroids on day 7. ARNIPL and ARV+Ni exhibited a significantly reduced number of alive cells compared to control, Ni and ARV (Figure 25). Moreover, Ni also showed decreased cell viability in co-culture spheroids compared to control.

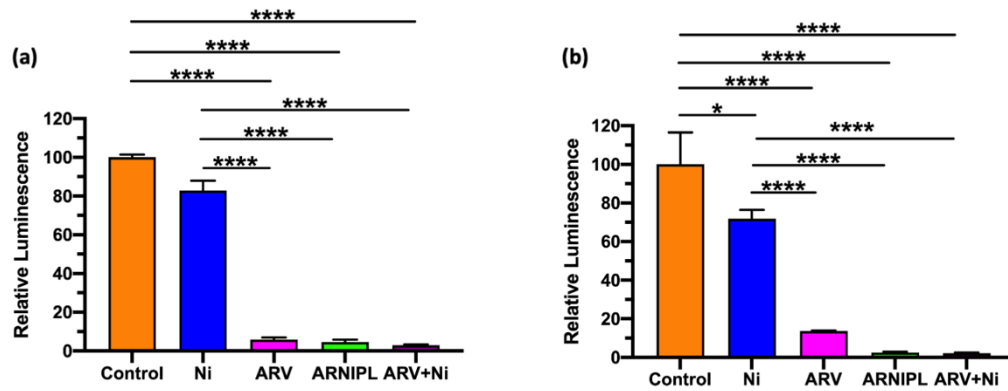


Figure 25. 3D cell viability assay conducted using CellTiter-Glo® kit. Results of various treatments in (a) A375R and (b) Co-culture 3D spheroids are shown as relative luminescence that normalized to control (100%). (*p < 0.05, ****p < 0.0001).

4.4.10.3 3D spheroid live & dead cell imaging

The fluorescent images of the dead cells and nuclei were taken on day 7. The red fluorescence obtained from ethidium homodimer-1 represents dead cells in the spheroids while blue color stained by DAPI represent cell nuclei. Green fluorescence was shown by GFP-labeled fibroblasts. Figure 26 showed the spheroids treated with ARV, ARNIPL and ARV+Ni had higher red intensity compared to control and Ni group. ARV and ARNIPL treated groups exhibited stronger red fluorescent intensity indicating higher killing of melanoma cells. In the co-culture model, the green fluorescent signal can be observed on the surface of the spheroids with Ni treatment whereas other groups showed faint green fluorescence and cannot be seen clearly after merging. This could be attribute to the inhibition growth of melanoma cells with Ni treatment. Similarly, ARV+Ni treated group also showed some extent green fluorescence on the surface of the spheroids. ARV, ARNIPL and ARV+Ni treated groups showed strong red intensity representing the dead cells. Moreover, the spheroids size of control is the largest, however, only the center that stained with nuclei dye can be seen, whereas spheroids with Ni treatment showed green fluorescence on the whole surface of the spheroids. This may due to the aggressive growth of melanoma cells were covered by the fibroblasts in the control group, on the other side, melanoma cells could be inhibited with Ni treatment so that the fluorescent fibroblasts covered the surface of the spheroids.

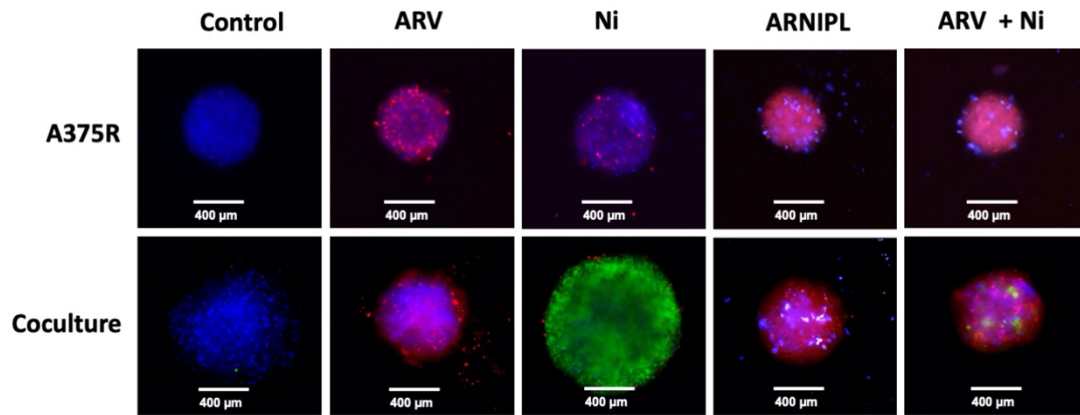


Figure 26. A375R and coculture 3D spheroids live & dead cell imaging on day 6. Spheroids were stained with DAPI (blue) for nuclei, EthD-1 (red) for compromised/dead cells, green fluorescence was shown by GFP-labeled fibroblasts. Representative images were taken at 20X magnification.

5 Limitations

The main objective is to develop nanoliposomes for the treatment of BRAF-mutant metastatic melanoma. In the first part of the thesis, active targeting PEGylated nanoliposomes (YTPL) were developed to target overexpressed EphA2 receptor in melanoma cell lines. However, we observed that expression of EphA2 receptor is relatively low in Vem resistant melanoma and uptake of YTPL was also lower in resistant melanoma cell compared to parent cells. Thus, YSA targeted liposomes could be helpful in melanoma but not in Vem resistant melanoma. Moreover, Vem resistant melanoma is also cross-resistance to MEK inhibitor. In second part we investigated effect of combination of a novel PROTAC molecule ARV-825 and anti-fibrotic agent Nintedanib in Vem resistant melanoma. Further, a nanoliposomes of ARV and NIN (ARNIPL) was developed, characterized and tested using various cytotoxicity assay. Nevertheless, there are some limitations as following:

- ARNIPL was found to be stable for one month in liquid form, however, the long-term stability could not be possible without freeze drying.
- Stroma-targeting strategy is helpful to enhance the uptake of therapeutics; however, it could be unpredictable whether modulating the ECM and stromal components of solid tumors will promote tumor metastasis and progression. Further *in-vivo* study and more considerations like administration time, sequence need to be investigated to achieve therapeutic benefit.
- PROTACs showed Hook effect at a higher concentration and it may eliminate the targeted protein sub-stoichiometrically. Additionally, Ni showed therapeutic effect only

above certain concentration. Thus, dose determination of is crucial and need to be thoroughly explored.

- There is possibility that melanoma cell become resistant to ARV and/or Ni similar to Vem therapy. We might evaluate it in future.
- The mechanism and the effect of Ni and ARV on fibroblasts in the 3D spheroids need to be further explored.

6 Summary

EphA2-Receptor Targeted PEGylated Nanoliposomes for the Treatment of BRAF^{V600E} Mutated Parent and Resistant Melanoma

As per our published work [125].

- Modified hydration showed higher entrapment efficiency of TMB than traditional thin film hydration method.
- The stability of TPL was enhanced using 10% trehalose as a cryoprotectant in the freeze drying.
- Differential scanning calorimetry (DSC) study confirmed that TMB was retained in a solubilized state within lipid bilayers.
- The drug release study showed TPL did not leak or burst release in 24 h.
- The hemolysis observed was negligible at therapeutic concentrations of TMB.
- Liposome showed higher intracellular uptake in parental cell lines compared to vemurafenib-resistant cell lines.
- Western blot analysis and a cytotoxicity study with the EphA2 inhibitor confirmed a reduction in EphA2 expression in resistant cell lines.

Thus, EphA2 receptor-targeted nanoliposomes can be useful for metastatic melanoma-specific delivery of TMB.

Development of Dual ARV-825 and Nintedanib - Loaded Nano-liposome for synergistic efficacy in Vemurafenib-resistant Melanoma

- A significant increasing amount TGF- β 1 was found in the vemurafenib-resistant melanoma cell lines compared to melanoma cell lines, which suggested the potential of targeting TGF β 1 in vemurafenib-resistant melanoma
- PROTAC molecule ARV and anti-fibrotic agent Ni exhibited synergistically in killing resistant melanoma cells. ARNIPL also remain the similar synergistic of cytotoxicity in resistant melanoma cells
- Entrapment efficiency, drug loading and stability of ARV and Ni in the ARNIPL were enhanced with the incorporation of citric acid.
- The drug release study showed ARNIPL did not leak or burst release in 48 h.
- ARNIPL showed significant higher population of early/late apoptosis after 24h treatment.
- ARNIPL demonstrated significant inhibition of vasculogenic mimicry and clonogenic effect in A375R.
- 3D multicellular tumor spheroids showed ARNIPL has promising inhibition effect in terms of tumor growth.

Hence, ARNIPL has encouraging indication for the treatment of vemurafenib-resistant melanoma as an alternative strategy by targeting to both cancer cells and tumor microenvironment.

7 Significance and future perspectives

This thesis provides two potential therapeutic approaches for the treatment of BRAF-mutant metastatic melanoma. The first perspective is based on the current problems associated with MEK inhibitor based targeted therapy. In order to minimize the side effects of MEKi trametinib, active targeting PEGylated nanoliposomes YTPL were successfully developed by leveraging both passive targeting and active targeting of nanoliposomes. Moreover, considering the reduced EphA2 expression in vemurafenib-resistant cell lines as well as cross-resistance to the MEKi, the second perspective focuses on exploring novel drug combinations using PROTAC molecule ARV-825 and anti-fibrotic agent Nintedanib, PROTAC molecule ARV. The combination effect of ARV and Ni was investigated for the first time in vemurafenib-resistant melanoma. ARNIPL was successfully developed using modified hydration method, where ARV and Ni exhibited synergism in killing vemurafenib-resistant melanoma cells in-vitro and strong tumor-suppressive effect in 3D spheroid model. Considering the importance and promising outcomes of this thesis, the following points could be done for the future research:

- Molecular mechanism behind ARV and Ni synergism
- Possibility of resistance development to ARV and Ni treatment
- Freeze-drying of ARNIPL
- Anticancer efficacy testing of ARNIPL in vemurafenib-resistant melanoma tumor bearing mice will be carried out check whether Ni treatment enhanced uptake of ARV liposome.

REFERENCES

1. Mathur, P.; Sathishkumar, K.; Chaturvedi, M.; Das, P.; Sudarshan, K.L.; Santhappan, S.; Nallasamy, V.; John, A.; Narasimhan, S.; Roselind, F.S. Cancer Statistics, 2020: Report From National Cancer Registry Programme, India. *JCO Global Oncology* **2020**, *6*, 1063-1075.
2. Liu, Q.; Das, M.; Liu, Y.; Huang, L. Targeted drug delivery to melanoma. *Advanced Drug Delivery Reviews* **2018**, *127*, 208-221.
3. Shain, A.H.; Bastian, B.C. From melanocytes to melanomas. *nature reviews Cancer* **2016**, *16*, 345.
4. Broekaert, S.M.; Roy, R.; Okamoto, I.; Van Den Oord, J.; Bauer, J.; Garbe, C.; Barnhill, R.L.; Busam, K.J.; Cochran, A.J.; Cook, M.G. Genetic and morphologic features for melanoma classification. *Pigment cell & melanoma research* **2010**, *23*, 763-770.
5. Cheng, L.; Lopez-Beltran, A.; Massari, F.; MacLennan, G.T.; Montironi, R. Molecular testing for BRAF mutations to inform melanoma treatment decisions: a move toward precision medicine. *Modern Pathology* **2018**, *31*, 24-38.
6. Amanuel, B.; Grieu, F.; Kular, J.; Millward, M.; Iacopetta, B. Incidence of BRAF p. Val600Glu and p. Val600Lys mutations in a consecutive series of 183 metastatic melanoma patients from a high incidence region. *Pathology* **2012**, *44*, 357-359.
7. Reddy, B.Y.; Miller, D.M.; Tsao, H. Somatic driver mutations in melanoma. *Cancer* **2017**, *123*, 2104-2117.
8. Amaral, T.; Sinnberg, T.; Meier, F.; Krepler, C.; Levesque, M.; Niessner, H.; Garbe, C. The mitogen-activated protein kinase pathway in melanoma part I - Activation and primary resistance mechanisms to BRAF inhibition. *Eur J Cancer* **2017**, *73*, 85-92, doi:10.1016/j.ejca.2016.12.010.
9. Leonardi, G.C.; Falzone, L.; Salemi, R.; Zanghi, A.; Spandidos, D.A.; McCubrey, J.A.; Candido, S.; Libra, M. Cutaneous melanoma: From pathogenesis to therapy (Review). *Int J Oncol* **2018**, *52*, 1071-1080, doi:10.3892/ijo.2018.4287.
10. Davis, L.E.; Shalin, S.C.; Tackett, A.J. Current state of melanoma diagnosis and treatment. *Cancer Biology & Therapy* **2019**, *20*, 1366-1379.
11. Lev, D.C.; Melinkova, V.O.; Onn, A.; Miller, C.; Stone, V.; Ruiz, M.; McGary, E.C.; Ananthaswamy, H.N.; Price, J.E.; Bar-Eli, M. Exposure of melanoma cells to dacarbazine results in enhanced tumor growth and metastasis in vivo. *AACR*: 2004.
12. Rotte, A. Combination of CTLA-4 and PD-1 blockers for treatment of cancer. *Journal of Experimental & Clinical Cancer Research* **2019**, *38*, 255.
13. Gu, L.; Khadaroo, P.A.; Su, H.; Kong, L.; Chen, L.; Wang, X.; Li, X.; Zhu, H.; Zhong, X.; Pan, J., et al. The safety and tolerability of combined immune checkpoint inhibitors (anti-PD-1/PD-L1 plus anti-CTLA-4): a systematic review and meta-analysis. *BMC Cancer* **2019**, *19*, 559, doi:10.1186/s12885-019-5785-z.
14. Achkar, T.; Tarhini, A.A. The use of immunotherapy in the treatment of melanoma. *Journal of hematology & oncology* **2017**, *10*, 88.
15. Domingues, B.; Lopes, J.M.; Soares, P.; Pópulo, H. Melanoma treatment in review. *ImmunoTargets and therapy* **2018**, *7*, 35.

16. Flaherty, K.T.; Puzanov, I.; Kim, K.B.; Ribas, A.; McArthur, G.A.; Sosman, J.A.; O'Dwyer, P.J.; Lee, R.J.; Grippo, J.F.; Nolop, K. Inhibition of mutated, activated BRAF in metastatic melanoma. *New England Journal of Medicine* **2010**, *363*, 809-819.
17. Sanchez, J.N.; Wang, T.; Cohen, M.S. BRAF and MEK inhibitors: use and resistance in BRAF-mutated cancers. *Drugs* **2018**, *78*, 549-566.
18. Kakadia, S.; Yarlagadda, N.; Awad, R.; Kundranda, M.; Niu, J.; Naraev, B.; Mina, L.; Dragovich, T.; Gimbel, M.; Mahmoud, F. Mechanisms of resistance to BRAF and MEK inhibitors and clinical update of US Food and Drug Administration-approved targeted therapy in advanced melanoma. *OncoTargets and therapy* **2018**, *11*, 7095.
19. Manzano, J.L.; Layos, L.; Buges, C.; de los Llanos Gil, M.; Vila, L.; Martinez-Balibrea, E.; Martinez-Cardus, A. Resistant mechanisms to BRAF inhibitors in melanoma. *Annals of translational medicine* **2016**, *4*.
20. Welsh, S.J.; Rizos, H.; Scolyer, R.A.; Long, G.V. Resistance to combination BRAF and MEK inhibition in metastatic melanoma: where to next? *European journal of cancer* **2016**, *62*, 76-85.
21. Flaherty, K.T.; Infante, J.R.; Daud, A.; Gonzalez, R.; Kefford, R.F.; Sosman, J.; Hamid, O.; Schuchter, L.; Cebon, J.; Ibrahim, N. Combined BRAF and MEK inhibition in melanoma with BRAF V600 mutations. *New England Journal of Medicine* **2012**, *367*, 1694-1703.
22. Flaherty, K.T.; Robert, C.; Hersey, P.; Nathan, P.; Garbe, C.; Milhem, M.; Demidov, L.V.; Hassel, J.C.; Rutkowski, P.; Mohr, P. Improved survival with MEK inhibition in BRAF-mutated melanoma. *New England Journal of Medicine* **2012**, *367*, 107-114.
23. Welsh, S.J.; Corrie, P.G. Management of BRAF and MEK inhibitor toxicities in patients with metastatic melanoma. *Therapeutic advances in medical oncology* **2015**, *7*, 122-136.
24. Banks, M.; Crowell, K.; Proctor, A.; Jensen, B.C. Cardiovascular Effects of the MEK Inhibitor, Trametinib: A Case Report, Literature Review, and Consideration of Mechanism. *Cardiovasc Toxicol* **2017**, *17*, 487-493, doi:10.1007/s12012-017-9425-z.
25. Pavlick, A.C.; Fecher, L.; Ascierto, P.A.; Sullivan, R.J. Frontline therapy for BRAF-mutated metastatic melanoma: how do you choose, and is there one correct answer? *American Society of Clinical Oncology Educational Book* **2019**, *39*, 564-571.
26. Wilmott, J.S.; Hersey, P.; Long, G.V.; Scolyer, R.A. Synergistic effects of MAPK and immune checkpoint inhibitors in melanoma: what is the best combination strategy? *Melanoma management* **2015**, *2*, 15-19.
27. Ziogas, D.C.; Konstantinou, F.; Bouros, S.; Gogas, H. Identifying the optimum first-line therapy in BRAF-mutant metastatic melanoma. *Expert Review of Anticancer Therapy* **2020**, *20*, 53-62.
28. Ruitter, D.; Bogenrieder, T.; Elder, D.; Herlyn, M. Melanoma–stroma interactions: structural and functional aspects. *The lancet oncology* **2002**, *3*, 35-43.
29. Lee, J.T.; Herlyn, M. Microenvironmental influences in melanoma progression. *Journal of cellular biochemistry* **2007**, *101*, 862-872.

30. Kalluri, R. The biology and function of fibroblasts in cancer. *Nature Reviews Cancer* **2016**, *16*, 582.
31. Li, G.; Satyamoorthy, K.; Meier, F.; Berking, C.; Bogenrieder, T.; Herlyn, M. Function and regulation of melanoma–stromal fibroblast interactions: when seeds meet soil. *Oncogene* **2003**, *22*, 3162-3171.
32. Erdogan, B.; Webb, D.J. Cancer-associated fibroblasts modulate growth factor signaling and extracellular matrix remodeling to regulate tumor metastasis. *Biochem Soc Trans* **2017**, *45*, 229-236, doi:10.1042/BST20160387.
33. Zeltz, C.; Primac, I.; Erusappan, P.; Alam, J.; Noel, A.; Gullberg, D. Cancer-associated fibroblasts in desmoplastic tumors: emerging role of integrins. In *Proceedings of Seminars in cancer biology*; pp. 166-181.
34. Wei, S.C.; Fattet, L.; Tsai, J.H.; Guo, Y.; Pai, V.H.; Majeski, H.E.; Chen, A.C.; Sah, R.L.; Taylor, S.S.; Engler, A.J. Matrix stiffness drives epithelial–mesenchymal transition and tumour metastasis through a TWIST1–G3BP2 mechanotransduction pathway. *Nature cell biology* **2015**, *17*, 678-688.
35. Tzanakakis, G.; Kavasi, R.M.; Voudouri, K.; Berdiaki, A.; Spyridaki, I.; Tsatsakis, A.; Nikitovic, D. Role of the extracellular matrix in cancer-associated epithelial to mesenchymal transition phenomenon. *Developmental Dynamics* **2018**, *247*, 368-381.
36. Fernandes, C.; Soares, D.; Yergeri, M.C. Tumor microenvironment targeted nanotherapy. *Frontiers in pharmacology* **2018**, *9*, 1230.
37. Bulbake, U.; Doppalapudi, S.; Kommineni, N.; Khan, W. Liposomal formulations in clinical use: an updated review. *Pharmaceutics* **2017**, *9*, 12.
38. Mohan, A.; Narayanan, S.; Balasubramanian, G.; Sethuraman, S.; Krishnan, U.M. Dual drug loaded nanoliposomal chemotherapy: A promising strategy for treatment of head and neck squamous cell carcinoma. *European Journal of Pharmaceutics and Biopharmaceutics* **2016**, *99*, 73-83.
39. Lasic, D.; Joannic, R.; Keller, B.; Frederik, P.; Auvray, L. Spontaneous vesiculation. *Advances in colloid and interface science* **2001**, *89*, 337-349.
40. Shaikh, I.M.; Tan, K.-B.; Chaudhury, A.; Liu, Y.; Tan, B.-J.; Tan, B.M.; Chiu, G.N. Liposome co-encapsulation of synergistic combination of irinotecan and doxorubicin for the treatment of intraperitoneally grown ovarian tumor xenograft. *Journal of Controlled Release* **2013**, *172*, 852-861.
41. Sen, K.; Banerjee, S.; Mandal, M. Dual drug loaded liposome bearing apigenin and 5-Fluorouracil for synergistic therapeutic efficacy in colorectal cancer. *Colloids and Surfaces B: Biointerfaces* **2019**, *180*, 9-22.
42. Vahed, S.Z.; Salehi, R.; Davaran, S.; Sharifi, S. Liposome-based drug co-delivery systems in cancer cells. *Materials Science and Engineering: C* **2017**, *71*, 1327-1341.
43. Jain, R.K.; Stylianopoulos, T. Delivering nanomedicine to solid tumors. *Nature reviews Clinical oncology* **2010**, *7*, 653.
44. Golombek, S.K.; May, J.N.; Theek, B.; Appold, L.; Drude, N.; Kiessling, F.; Lammers, T. Tumor targeting via EPR: Strategies to enhance patient responses. *Adv Drug Deliv Rev* **2018**, *130*, 17-38, doi:10.1016/j.addr.2018.07.007.

45. Immordino, M.L.; Dosio, F.; Cattel, L. Stealth liposomes: review of the basic science, rationale, and clinical applications, existing and potential. *Int J Nanomedicine* **2006**, *1*, 297-315.
46. Bertrand, N.; Wu, J.; Xu, X.; Kamaly, N.; Farokhzad, O.C. Cancer nanotechnology: the impact of passive and active targeting in the era of modern cancer biology. *Advanced drug delivery reviews* **2014**, *66*, 2-25.
47. Danhier, F.; Feron, O.; Préat, V. To exploit the tumor microenvironment: passive and active tumor targeting of nanocarriers for anti-cancer drug delivery. *Journal of controlled release* **2010**, *148*, 135-146.
48. Zylberberg, C.; Matosevic, S. Pharmaceutical liposomal drug delivery: a review of new delivery systems and a look at the regulatory landscape. *Drug Delivery* **2016**, *23*, 3319-3329.
49. Sercombe, L.; Veerati, T.; Moheimani, F.; Wu, S.Y.; Sood, A.K.; Hua, S. Advances and challenges of liposome assisted drug delivery. *Frontiers in pharmacology* **2015**, *6*, 286.
50. Long, G.V.; Stroyakovskiy, D.; Gogas, H.; Levchenko, E.; de Braud, F.; Larkin, J.; Garbe, C.; Jouary, T.; Hauschild, A.; Grob, J.J. Combined BRAF and MEK inhibition versus BRAF inhibition alone in melanoma. *New England Journal of Medicine* **2014**, *371*, 1877-1888.
51. Lugowska, I.; Kosela-Paterczyk, H.; Kozak, K.; Rutkowski, P. Trametinib: a MEK inhibitor for management of metastatic melanoma. *Oncotargets and therapy* **2015**, *8*, 2251.
52. Duncan, K.; Chang, L.; Patronas, M. MEK inhibitors: a new class of chemotherapeutic agents with ocular toxicity. *Eye* **2015**, *29*, 1003-1012.
53. Chapman, P.B.; Hauschild, A.; Robert, C.; Haanen, J.B.; Ascierto, P.; Larkin, J.; Dummer, R.; Garbe, C.; Testori, A.; Maio, M. Improved survival with vemurafenib in melanoma with BRAF V600E mutation. *New England Journal of Medicine* **2011**, *364*, 2507-2516.
54. Villanueva, J.; Vultur, A.; Herlyn, M. Resistance to BRAF inhibitors: unraveling mechanisms and future treatment options. *Cancer Res* **2011**, *71*, 7137-7140, doi:10.1158/0008-5472.CAN-11-1243.
55. Gowrishankar, K.; Snoyman, S.; Pupo, G.M.; Becker, T.M.; Kefford, R.F.; Rizos, H. Acquired resistance to BRAF inhibition can confer cross-resistance to combined BRAF/MEK inhibition. *J Invest Dermatol* **2012**, *132*, 1850-1859, doi:10.1038/jid.2012.63.
56. Luebker, S.A.; Koepsell, S.A. Diverse mechanisms of BRAF inhibitor resistance in melanoma identified in clinical and preclinical studies. *Frontiers in oncology* **2019**, *9*, 268.
57. Torres-Collado, A.X.; Knott, J.; Jazirehi, A.R. Reversal of Resistance in Targeted Therapy of Metastatic Melanoma: Lessons Learned from Vemurafenib (BRAF(V600E)-Specific Inhibitor). *Cancers (Basel)* **2018**, *10*, doi:10.3390/cancers10060157.
58. Rossi, A.; Roberto, M.; Panebianco, M.; Botticelli, A.; Mazzuca, F.; Marchetti, P. Drug resistance of BRAF-mutant melanoma: Review of up-to-date mechanisms of action and promising targeted agents. *European journal of pharmacology* **2019**, *862*, 172621.

59. Rollins, R.A.; Kim, K.H.; Tsao, C.C. The Emerging Epigenetic Landscape in Melanoma. *Human Skin Cancer, Potential Biomarkers and Therapeutic Targets* **2016**, *9*.
60. Sarkar, D.; Leung, E.Y.; Baguley, B.C.; Finlay, G.J.; Askarian-Amiri, M.E. Epigenetic regulation in human melanoma: past and future. *Epigenetics* **2015**, *10*, 103-121, doi:10.1080/15592294.2014.1003746.
61. Lin, X.; Sun, R.; Zhao, X.; Zhu, D.; Zhao, X.; Gu, Q.; Dong, X.; Zhang, D.; Zhang, Y.; Li, Y., et al. C-myc overexpression drives melanoma metastasis by promoting vasculogenic mimicry via c-myc/snail/Bax signaling. *J Mol Med (Berl)* **2017**, *95*, 53-67, doi:10.1007/s00109-016-1452-x.
62. Segura, M.F.; Fontanals-Cirera, B.; Gaziél-Sovran, A.; Guijarro, M.V.; Hanniford, D.; Zhang, G.; González-Gomez, P.; Morante, M.; Jubierre, L.; Zhang, W. BRD4 sustains melanoma proliferation and represents a new target for epigenetic therapy. *Cancer research* **2013**, *73*, 6264-6276.
63. Prochownik, E.V.; Vogt, P.K. Therapeutic Targeting of Myc. *Genes Cancer* **2010**, *1*, 650-659, doi:10.1177/1947601910377494.
64. Aird, F.; Kandela, I.; Mantis, C.; Reproducibility Project: Cancer, B. Replication Study: BET bromodomain inhibition as a therapeutic strategy to target c-Myc. *Elife* **2017**, *6*, doi:10.7554/eLife.21253.
65. Delmore, J.E.; Issa, G.C.; Lemieux, M.E.; Rahl, P.B.; Shi, J.; Jacobs, H.M.; Kastritis, E.; Gilpatrick, T.; Paranal, R.M.; Qi, J., et al. BET bromodomain inhibition as a therapeutic strategy to target c-Myc. *Cell* **2011**, *146*, 904-917, doi:10.1016/j.cell.2011.08.017.
66. Chen, H.; Liu, H.; Qing, G. Targeting oncogenic Myc as a strategy for cancer treatment. *Signal transduction and targeted therapy* **2018**, *3*, 1-7.
67. Shi, J.; Vakoc, C.R. The mechanisms behind the therapeutic activity of BET bromodomain inhibition. *Mol Cell* **2014**, *54*, 728-736, doi:10.1016/j.molcel.2014.05.016.
68. Wu, S.-Y.; Chiang, C.-M. The double bromodomain-containing chromatin adaptor Brd4 and transcriptional regulation. *Journal of Biological Chemistry* **2007**, *282*, 13141-13145.
69. Zhao, B.; Cheng, X.; Zhou, X. The BET-bromodomain inhibitor JQ1 mitigates vemurafenib drug resistance in melanoma. *Melanoma research* **2018**, *28*, 521.
70. Echevarría-Vargas, I.M.; Reyes-Uribe, P.I.; Guterres, A.N.; Yin, X.; Kossenkov, A.V.; Liu, Q.; Zhang, G.; Krepler, C.; Cheng, C.; Wei, Z. Co-targeting BET and MEK as salvage therapy for MAPK and checkpoint inhibitor-resistant melanoma. *EMBO molecular medicine* **2018**, *10*.
71. Tiago, M.; Capparelli, C.; Erkes, D.A.; Purwin, T.J.; Heilman, S.A.; Berger, A.C.; Davies, M.A.; Aplin, A.E. Targeting BRD/BET proteins inhibits adaptive kinome upregulation and enhances the effects of BRAF/MEK inhibitors in melanoma. *British Journal of Cancer* **2020**, 1-12.
72. Sakamoto, K.M.; Kim, K.B.; Kumagai, A.; Mercurio, F.; Crews, C.M.; Deshaies, R.J. Protacs: chimeric molecules that target proteins to the Skp1-Cullin-F box complex for ubiquitination and degradation. *Proc Natl Acad Sci U S A* **2001**, *98*, 8554-8559, doi:10.1073/pnas.141230798.

73. Cermakova, K.; Hodges, H.C. Next-Generation Drugs and Probes for Chromatin Biology: From Targeted Protein Degradation to Phase Separation. *Molecules* **2018**, *23*, doi:10.3390/molecules23081958.
74. Lu, J.; Qian, Y.; Altieri, M.; Dong, H.; Wang, J.; Raina, K.; Hines, J.; Winkler, J.D.; Crew, A.P.; Coleman, K. Hijacking the E3 ubiquitin ligase cereblon to efficiently target BRD4. *Chemistry & biology* **2015**, *22*, 755-763.
75. Rathod, D.; Fu, Y.; Patel, K. BRD4 PROTAC as a novel therapeutic approach for the treatment of vemurafenib resistant melanoma: preformulation studies, formulation development and in vitro evaluation. *European Journal of Pharmaceutical Sciences* **2019**, *138*, 105039.
76. Flach, E.H.; Rebecca, V.W.; Herlyn, M.; Smalley, K.S.; Anderson, A.R. Fibroblasts contribute to melanoma tumor growth and drug resistance. *Molecular pharmaceutics* **2011**, *8*, 2039-2049.
77. Wright, C.J.; McCormack, P.L. Trametinib: first global approval. *Drugs* **2013**, *73*, 1245-1254.
78. Yoshida, T.; Kakegawa, J.; Yamaguchi, T.; Hantani, Y.; Okajima, N.; Sakai, T.; Watanabe, Y.; Nakamura, M. Identification and characterization of a novel chemotype MEK inhibitor able to alter the phosphorylation state of MEK1/2. *Oncotarget* **2012**, *3*, 1533-1545, doi:10.18632/oncotarget.747.
79. Lugowska, I.; Kosela-Paterczyk, H.; Kozak, K.; Rutkowski, P. Trametinib: a MEK inhibitor for management of metastatic melanoma. *Onco Targets Ther* **2015**, *8*, 2251-2259, doi:10.2147/OTT.S72951.
80. Flaherty, K.T.; Infante, J.R.; Daud, A.; Gonzalez, R.; Kefford, R.F.; Sosman, J.; Hamid, O.; Schuchter, L.; Cebon, J.; Ibrahim, N., et al. Combined BRAF and MEK inhibition in melanoma with BRAF V600 mutations. *N Engl J Med* **2012**, *367*, 1694-1703, doi:10.1056/NEJMoa1210093.
81. King, J.W.; Nathan, P.D. Role of the MEK inhibitor trametinib in the treatment of metastatic melanoma. *Future Oncology* **2014**, *10*, 1559-1570.
82. Long, G.V.; Hauschild, A.; Santinami, M.; Atkinson, V.; Mandalà, M.; Chiarion-Sileni, V.; Larkin, J.; Nyakas, M.; Dutriaux, C.; Haydon, A. Adjuvant dabrafenib plus trametinib in stage III BRAF-mutated melanoma. *New England Journal of Medicine* **2017**, *377*, 1813-1823.
83. Committee, E.N. Unified nomenclature for Eph family receptors and their ligands, the ephrins. *Cell* **1997**, *90*, 403-404.
84. Udayakumar, D.; Zhang, G.; Ji, Z.; Njauw, C.-N.; Mroz, P.; Tsao, H. EphA2 is a critical oncogene in melanoma. *Oncogene* **2011**, *30*, 4921-4929.
85. Hendrix, M.J.; Seftor, E.A.; Seftor, R.E.; Chao, J.-T.; Chien, D.-S.; Chu, Y.-W. Tumor cell vascular mimicry: Novel targeting opportunity in melanoma. *Pharmacology & therapeutics* **2016**, *159*, 83-92.
86. Neill, T.; Buraschi, S.; Goyal, A.; Sharpe, C.; Natkanski, E.; Schaefer, L.; Morrione, A.; Iozzo, R.V. EphA2 is a functional receptor for the growth factor progranulin. *Journal of Cell Biology* **2016**, *215*, 687-703.
87. Tandon, M.; Vemula, S.V.; Mittal, S.K. Emerging strategies for EphA2 receptor targeting for cancer therapeutics. *Expert opinion on therapeutic targets* **2011**, *15*, 31-51.

88. Miao, B.; Ji, Z.; Tan, L.; Taylor, M.; Zhang, J.; Choi, H.G.; Frederick, D.T.; Kumar, R.; Wargo, J.A.; Flaherty, K.T. EphA2 is a mediator of vemurafenib resistance and a novel therapeutic target in melanoma. *Cancer discovery* **2015**, *5*, 274-287.
89. Wu, B.; Wang, S.; De, S.K.; Barile, E.; Quinn, B.A.; Zharkikh, I.; Purves, A.; Stebbins, J.L.; Oshima, R.G.; Fisher, P.B., et al. Design and Characterization of Novel EphA2 Agonists for Targeted Delivery of Chemotherapy to Cancer Cells. *Chem Biol* **2015**, *22*, 876-887, doi:10.1016/j.chembiol.2015.06.011.
90. Patel, K.; Doddapaneni, R.; Sekar, V.; Chowdhury, N.; Singh, M. Combination approach of YSA peptide anchored docetaxel stealth liposomes with oral antifibrotic agent for the treatment of lung cancer. *Molecular pharmaceuticals* **2016**, *13*, 2049-2058.
91. Ingvarsson, P.T.; Yang, M.; Nielsen, H.M.; Rantanen, J.; Foged, C. Stabilization of liposomes during drying. *Expert Opin Drug Deliv* **2011**, *8*, 375-388, doi:10.1517/17425247.2011.553219.
92. Wang, W. Lyophilization and development of solid protein pharmaceuticals. *International journal of pharmaceuticals* **2000**, *203*, 1-60.
93. Hedoux, A.; Paccou, L.; Achir, S.; Guinet, Y. Mechanism of protein stabilization by trehalose during freeze-drying analyzed by in situ micro-Raman spectroscopy. *Journal of Pharmaceutical Sciences* **2013**, *102*, 2484-2494.
94. Chen, C.; Han, D.; Cai, C.; Tang, X. An overview of liposome lyophilization and its future potential. *Journal of controlled release* **2010**, *142*, 299-311.
95. Zhang, L.; Liu, L.; Qian, Y.; Chen, Y. The effects of cryoprotectants on the freeze-drying of ibuprofen-loaded solid lipid microparticles (SLM). *European journal of pharmaceuticals and biopharmaceuticals* **2008**, *69*, 750-759.
96. Wei, X.; Patil, Y.; Ohana, P.; Amitay, Y.; Shmeeda, H.; Gabizon, A.; Barenholz, Y. Characterization of pegylated liposomal mitomycin C lipid-based prodrug (Promitil) by high sensitivity differential scanning calorimetry and cryogenic transmission electron microscopy. *Molecular pharmaceuticals* **2017**, *14*, 4339-4345.
97. Lipinski, C.A. Lead-and drug-like compounds: the rule-of-five revolution. *Drug Discovery Today: Technologies* **2004**, *1*, 337-341.
98. Chemistry, R.S.o. ARV-825. 2017; Vol. 2017.
99. Hilberg, F.; Tontsch-Grunt, U.; Baum, A.; Le, A.T.; Doebele, R.C.; Lieb, S.; Gianni, D.; Voss, T.; Garin-Chesa, P.; Haslinger, C. Triple angiokinase inhibitor nintedanib directly inhibits tumor cell growth and induces tumor shrinkage via blocking oncogenic receptor tyrosine kinases. *Journal of Pharmacology and Experimental Therapeutics* **2018**, *364*, 494-503.
100. Lin, X.; Wen, J.; Liu, R.; Gao, W.; Qu, B.; Yu, M. Nintedanib inhibits TGF- β -induced myofibroblast transdifferentiation in human Tenon's fibroblasts. *Molecular Vision* **2018**, *24*, 789.
101. Rangarajan, S.; Kurundkar, A.; Kurundkar, D.; Bernard, K.; Sanders, Y.Y.; Ding, Q.; Antony, V.B.; Zhang, J.; Zmijewski, J.; Thannickal, V.J. Novel mechanisms for the antifibrotic action of nintedanib. *American journal of respiratory cell and molecular biology* **2016**, *54*, 51-59.

102. Wind, S.; Schmid, U.; Freiwald, M.; Marzin, K.; Lotz, R.; Ebner, T.; Stopfer, P.; Dallinger, C. Clinical pharmacokinetics and pharmacodynamics of nintedanib. *Clinical pharmacokinetics* **2019**, 1-17.
103. Herbertz, S.; Sawyer, J.S.; Stauber, A.J.; Gueorguieva, I.; Driscoll, K.E.; Estrem, S.T.; Cleverly, A.L.; Desai, D.; Guba, S.C.; Benhadji, K.A., et al. Clinical development of galunisertib (LY2157299 monohydrate), a small molecule inhibitor of transforming growth factor-beta signaling pathway. *Drug Des Devel Ther* **2015**, *9*, 4479-4499, doi:10.2147/DDDT.S86621.
104. Santini, V.; Valcárcel, D.; Platzbecker, U.; Komrokji, R.S.; Cleverly, A.L.; Lahn, M.M.; Janssen, J.; Zhao, Y.; Chiang, A.; Giagounidis, A. Phase II study of the ALK5 inhibitor galunisertib in very low-, low-, and intermediate-risk myelodysplastic syndromes. *Clinical Cancer Research* **2019**, *25*, 6976-6985.
105. Luangmonkong, T.; Suriguga, S.; Bigaeva, E.; Boersema, M.; Oosterhuis, D.; de Jong, K.P.; Schuppan, D.; Mutsaers, H.A.M.; Olinga, P. Evaluating the antifibrotic potency of galunisertib in a human ex vivo model of liver fibrosis. *Br J Pharmacol* **2017**, *174*, 3107-3117, doi:10.1111/bph.13945.
106. Margaritopoulos, G.A.; Vasarmidi, E.; Antoniou, K.M. Pirfenidone in the treatment of idiopathic pulmonary fibrosis: an evidence-based review of its place in therapy. *Core Evid* **2016**, *11*, 11-22, doi:10.2147/CE.S76549.
107. Food, U.; Administration, D. FDA approves Esbriet to treat idiopathic pulmonary fibrosis. 2015.
108. Lin, X.; Yu, M.; Wu, K.; Yuan, H.; Zhong, H. Effects of pirfenidone on proliferation, migration, and collagen contraction of human Tenon's fibroblasts in vitro. *Investigative ophthalmology & visual science* **2009**, *50*, 3763-3770.
109. Conte, E.; Gili, E.; Fagone, E.; Fruciano, M.; Iemmolo, M.; Vancheri, C. Effect of pirfenidone on proliferation, TGF- β -induced myofibroblast differentiation and fibrogenic activity of primary human lung fibroblasts. *European Journal of Pharmaceutical Sciences* **2014**, *58*, 13-19.
110. Ruwanpura, S.M.; Thomas, B.J.; Bardin, P.G. Pirfenidone: Molecular Mechanisms and Potential Clinical Applications in Lung Disease. *American Journal of Respiratory Cell and Molecular Biology* **2020**, *62*, 413-422.
111. Lopez-de la Mora, D.A.; Sanchez-Roque, C.; Montoya-Buelna, M.; Sanchez-Enriquez, S.; Lucano-Landeros, S.; Macias-Barragan, J.; Armendariz-Borunda, J. Role and New Insights of Pirfenidone in Fibrotic Diseases. *Int J Med Sci* **2015**, *12*, 840-847, doi:10.7150/ijms.11579.
112. Li, X.; Song, Y. Proteolysis-targeting chimera (PROTAC) for targeted protein degradation and cancer therapy. *Journal of Hematology & Oncology* **2020**, *13*, 1-14.
113. Yang, S.T.; Kreutzberger, A.J.B.; Lee, J.; Kiessling, V.; Tamm, L.K. The role of cholesterol in membrane fusion. *Chem Phys Lipids* **2016**, *199*, 136-143, doi:10.1016/j.chemphyslip.2016.05.003.
114. Marques-Gallego, P.; de Kroon, A.I. Ligation strategies for targeting liposomal nanocarriers. *Biomed Res Int* **2014**, *2014*, 129458, doi:10.1155/2014/129458.
115. Spender, L.C.; Ferguson, G.J.; Liu, S.; Cui, C.; Girotti, M.R.; Sibbet, G.; Higgs, E.B.; Shuttleworth, M.K.; Hamilton, T.; Lorigan, P., et al. Mutational activation of BRAF confers sensitivity to transforming growth factor beta inhibitors in

- human cancer cells. *Oncotarget* **2016**, *7*, 81995-82012, doi:10.18632/oncotarget.13226.
116. Maniotis, A.J.; Folberg, R.; Hess, A.; Seftor, E.A.; Gardner, L.M.; Pe'er, J.; Trent, J.M.; Meltzer, P.S.; Hendrix, M.J. Vascular channel formation by human melanoma cells in vivo and in vitro: vasculogenic mimicry. *The American journal of pathology* **1999**, *155*, 739-752.
117. Folberg, R.; Hendrix, M.J.; Maniotis, A.J. Vasculogenic mimicry and tumor angiogenesis. *The American journal of pathology* **2000**, *156*, 361-381.
118. Fu, Y.; Rathod, D.; Patel, K. Protein kinase C inhibitor anchored BRD4 PROTAC PEGylated nanoliposomes for the treatment of vemurafenib-resistant melanoma. *Exp Cell Res* **2020**, *396*, 112275, doi:10.1016/j.yexcr.2020.112275.
119. Zhang, X.; Zhang, J.; Zhou, H.; Fan, G.; Li, Q. Molecular Mechanisms and Anticancer Therapeutic Strategies in Vasculogenic Mimicry. *J Cancer* **2019**, *10*, 6327-6340, doi:10.7150/jca.34171.
120. Sahni, J.M.; Gayle, S.S.; Bonk, K.L.; Vite, L.C.; Yori, J.L.; Webb, B.; Ramos, E.K.; Seachrist, D.D.; Landis, M.D.; Chang, J.C., et al. Bromodomain and Extraterminal Protein Inhibition Blocks Growth of Triple-negative Breast Cancers through the Suppression of Aurora Kinases. *J Biol Chem* **2016**, *291*, 23756-23768, doi:10.1074/jbc.M116.738666.
121. Berenguer-Daize, C.; Astorgues-Xerri, L.; Odore, E.; Cayol, M.; Cvitkovic, E.; Noel, K.; Bekradda, M.; MacKenzie, S.; Rezai, K.; Lokiec, F., et al. OTX015 (MK-8628), a novel BET inhibitor, displays in vitro and in vivo antitumor effects alone and in combination with conventional therapies in glioblastoma models. *Int J Cancer* **2016**, *139*, 2047-2055, doi:10.1002/ijc.30256.
122. Jeong, S.Y.; Lee, J.H.; Shin, Y.; Chung, S.; Kuh, H.J. Co-Culture of Tumor Spheroids and Fibroblasts in a Collagen Matrix-Incorporated Microfluidic Chip Mimics Reciprocal Activation in Solid Tumor Microenvironment. *PLoS One* **2016**, *11*, e0159013, doi:10.1371/journal.pone.0159013.
123. Jeong, S.-Y.; Lee, J.-H.; Shin, Y.; Chung, S.; Kuh, H.-J. Co-culture of tumor spheroids and fibroblasts in a collagen matrix-incorporated microfluidic chip mimics reciprocal activation in solid tumor microenvironment. *PloS one* **2016**, *11*, e0159013.
124. Saraswat, A.; Patki, M.; Fu, Y.; Barot, S.; Dukhande, V.V.; Patel, K. Nanoformulation of PROteolysis TArgeting Chimera targeting 'undruggable' c-Myc for the treatment of pancreatic cancer. *Nanomedicine (Lond)* **2020**, *15*, 1761-1777, doi:10.2217/nnm-2020-0156.
125. Fu, Y.; Rathod, D.; Abo-Ali, E.M.; Dukhande, V.V.; Patel, K. EphA2-Receptor Targeted PEGylated Nanoliposomes for the Treatment of BRAFV600E Mutated Parent-and Vemurafenib-Resistant Melanoma. *Pharmaceutics* **2019**, *11*, 504.

VITA

Name	Yige Fu
Middle School	Attached Middle School to Jilin University, Changchun, China.
Date Graduated	July 2008.
High School	High School Attached to Northeast Normal University, Changchun, China.
Date Graduated	July 2011.
Bachelor of Science	Jilin University, Changchun, China. Major: Pharmaceutics
Date Graduated	May 2015.